CZECH TECHNICAL UNIVERSITY IN PRAGUE
FACULTY OF MECHANICAL ENGINEERING
DEPARTMENT OF ENVIRONMENTAL ENGINEERING

GEOMETRY OF TUBE RADIANT HEATERS

DIPLOMA THESIS

Bc. Noémi BELEY 1 – EE – 2016

Czech Technical University in Prague
Faculty of Mechanical Engineering

Department of Environmental Engineering Academic year: **2015/2016**

MASTER THESIS ASSIGNMENT

Student name: **Bc. Noémi BELEY**

Study program: **Mechanical Engineering**

Study field: **Environmental Engineering**

Thesis title: **Geometry of Tube Radiant Heaters**

Elaboration guidelines:

Analyze the influence of tube radiant heater geometry on the distribution of emitted heat radiation. The study will be based on numerical simulations with discrete ordinates (DO) model. Test the model sensitivity to surface splitting, angle discretization and density of numerical grid. Find a suitable method for the evaluation of heat radiation intensity generated by tube radiant heaters. Apply this method to compare different geometrical configurations of heat emitting tubes and reflectors.

Extent of graphic work: Graphic presentation of the results.

Extent of textual report: Detailed technical report including the description of applied methods and the discussion of results.

Literature:

1) Siegel R., Howell J. *Thermal Radiation Heat Transfer.* 4th ed. Taylor & Francis, New York, 2002.
2) Modest M. F. *Radiative Heat Transfer.* 2nd ed. Academic Press, London, 2003.
3) *ANSYS Documentation, Release 16.2.* ANSYS Inc., Canonsburg, 2015.

Thesis supervisor: **Ing. Martin Barták, Ph.D.**

Consultant: -

Assignment issue date: **30.10. 2015**

Thesis due date: **12.1. 2016**

If the student does not submit his/her thesis by the due date and provides a reasonable excuse in writing, and the excuse is accepted by the dean, the dean appoints a substitute deadline for the thesis submission. If the student does not deliver a proper letter of excuse or if the excuse is not accepted by the dean, the student is eligible for a second thesis enrolment.

The student is aware that the thesis has to be accomplished through an independent and unassisted student's work, supported only by recognized consultations. Literature and other information resources as well as consultants' names have to be acknowledged in the thesis.

Thesis assignment received: 30/10/2015 (Date) ..... (Student)

Doc. Ing. Vladimír Zmrhal, Ph.D.
Head of the Department

ČESKÉ VYSOKÉ UČENÍ TECHNICKÉ V PRAZE Fakulta strojní

Prof. Ing. Michael Valášek, DrSc.
Dean of the Faculty

Prague, 30.10. 2015

Abstract

The thesis deals with the tube radiant heater geometry and the impact of a heater reflector on the distribution of radiation intensity emitted into the heated space. The analysis is based on simulations in ANSYS Fluent using the discrete ordinates (DO) model for radiation. Some preliminary tests were conducted to decide about the model configuration. The attention was paid particularly to the angle discretization in the DO model and to the density of the computational mesh. An important finding from the preliminary tests is that it is necessary to couple DO model with energy transfer simulations (a standalone simulation of radiation does not provide reasonable results). A method was then formulated and applied to compare seven geometries of heater reflectors found from different manufacturers. This was done by comparing the radiative heat flux repartition on the control boundary. Two repartitions are considered: based on the useful angle of the heater and based on the left/right partition. The best heater when combining the two considerations was the model Schwank 50U.

Keywords: radiative heat transfer, tube radiant heater, DO model, simulation, ANSYS Fluent

Abstrakt

Geometrie tmavých plynových zářičů

Diplomová práce se zabývá geometrií tmavých zářičů a vlivem reflektoru zářiče na distribuci intensity záření do vytápěného prostoru. Analýza je založena na simulacích v programu ANSYS Fluent s užitím DO modelu pro záření. Bylo provedeny předběžné testy za účelem stanovit konfiguraci modelu. Pozornost byla věnována zvláště úhlové diskretizaci a hustotě výpočetní sítě. Důležitým poznatkem z těchto testů je, že DO model je nutné používat v propojení se simulací přenosu energie (simulace se samotným DO model neposkytuje přijatelné výsledky). Dále byla formulována a použita metoda pro porovnání sedmi geometrií reflektorů od různých výrobců. To bylo provedeno porovnáním rozdělení sálavého tepelného toku na kontrolní hranici. Bylo uvažováno rozdělení s ohledem na využitelný úhel zářiče a na levou/pravou část zářiče. V kombinaci těchto dvou kritérií vyšel jako nejlepší model Schwank 50U.

Klíčová slova: přenos tepla sáláním, tmavý plynový zářič, DO model, simulace, ANSYS Fluent

Statement

I declare that this diploma thesis entitled "Geometry of Tube Radiant Heaters" is my own work performed under the supervision of Ing. Martin Barták, Ph.D., with the use of the literature presented at the end of my diploma thesis in the list of references.

In Prague, 11/01/2016, Noémi Beley

Table of Contents

Symbols and units

Symbol	**Meaning**	**Unit**
a	Absorption coefficient	m^{-1}
e	Emissive power	W/m^2
I	Intensity of radiation or radiative intensity	W/m^2
s	Geometric path length	m
T	Thermodynamic temperature	K
ε	Emissivity	-
λ	Wavelength	m
μ_s	Scattering coefficient	m^{-1}
σ	Stefan-Boltzmann constant	$W/m^2.K^4$

1. Introduction

Radiative heat transfer is used for heating mainly in large spaces (warehouses, hangars) where convective heaters are not effective enough. Tube radiant heaters are gas-fired infrared heating devices. They are mainly composed of a gas burner creating a flame inside a tube, and a reflector above the tube to direct the heat radiation produced.

Several factors have a role in tube radiant heater design, for example tube and reflector materials, burner and exhaust system designs, insulation, or reflector geometry. The reflector geometry has an important impact on the effectiveness of the heater as it influences the proportion of the produced heat that is delivered to the occupants' area. This study is conducted to analyse the influence of tube radiant heater geometry on the distribution of emitted heat radiation. It focuses on the reflector geometry. Several different geometries from real heaters available on the market are compared.

This analysis is based on numerical simulations using the CFD-software ANSYS Fluent. This software provides several models to include radiation in heat transfer simulations. Being the only one suitable for this study, the discrete ordinates (DO) model is used. Only a 2D-view of the radiant heater is used in the simulations.

After giving some theoretical background, preliminary tests using two simple geometries are presented in Chapter 3. Their goals are to find the correct configuration in Fluent to be used for the simulations, and a suitable method for the evaluation of heat radiation in tube radiant heaters. The model sensitivity to the angle discretization of the DO model and to the density of the computational mesh is particularly studied. Then, some general information about tube radiant heaters is presented and the seven heater geometries used for the comparison are given in Chapter 4. The Chapter 5 presents the set up tests performed with a real heater geometry. They allow to make a final decision on the configuration and the method to be used. Finally in Chapter 6, the different geometries are compared using the radiative heat flux distribution on the control boundary. Two repartitions are considered: based on the useful angle of the heater and based on the left/right partition. The principal results are summarised in the conclusion.

2. Theoretical background

Three types of heat transfer exist: conduction, convection and radiation. Conduction occurs by means of molecular agitation within a material, without any motion of the material as a whole. Convection is the process of heat transfer from one location to the next by the movement of a fluid. Both of these means of heat transfer require the presence of some material (medium) in which the energy can be transferred.

Radiation however is the transfer of heat by means of electromagnetic waves, or photons. Unlike the two previous types, radiation heat transfer can occur through matter as well as in vacuum. It is especially significant at high temperature, or when natural convection occurs at low temperature so that radiation is of the same order of magnitude.

There is another important difference between radiation and the two other types of heat transfer. For both conduction and convection, at constant material properties, the heat transfer rate is linearly proportional to the temperature difference. On the other hand, for thermal radiation, it is generally proportional to the difference of thermodynamic temperatures to the fourth power.

2.1. Heat transfer by radiation

All bodies constantly emit electromagnetic waves and therefore thermal energy by radiation. The intensity of this emission depends on the temperature of the body and the nature of its surface.

Wavelength

Electromagnetic waves are characterised with their wavelength λ (m, usually expressed in µm) or their frequency ν (s^{-1} or Hz). These quantities are related following this formula.

$$\nu = \frac{c}{\lambda} \tag{1}$$

where c (m/s) is the speed of light.

A great range of wavelengths exists for electromagnetic waves but only a small part concerns thermal radiation: between 0.1 µm (ultraviolet) and 100 µm (mid infrared). It includes the visible light range which is between 0.4 and 0.7 µm.

Black body and grey body

When some radiative energy reaches a body, a part of it can be absorbed, another reflected and another transmitted through the body. A black body is a perfect absorber, which means that it does not reflect nor transmit anything, all the energy that reaches it is absorbed. This type of body is an ideal one. It is also a perfect emitter.

In reality, many surfaces can be approximated as grey bodies, which emit less than black bodies. A grey body is characterized principally by its emissivity or emittance ε which ranges between 0 and 1. The emissivity of a black body is 1. The grey body is also an approximation actually, for which the emissivity is the same for every wavelength. In reality, the monochromatic emissivity can be different from the total emissivity. For a diffuse solid surface and for a gas, the absorptance is equal to the emissivity, which means that as much radiation is emitted that it is absorbed.

Diffuse and specular radiation

When incident radiation comes in contact with a surface, it can be reflected. There are two types of reflection: diffuse and specular.

Reflection on smooth surfaces such as reflectors leads to a type of reflection known as specular reflection. Reflection on rough surfaces leads to a type of reflection known as diffuse reflection. The proportion of diffuse reflection occurring on a surface is characterized by the diffuse fraction f_d of the surface. The Figure 1 depicts two beams of radiation incident upon a rough and a smooth surface.

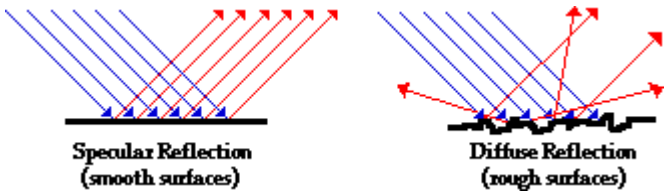

FIGURE 1. DIFFUSE AND SPECULAR REFLECTION [HENDERSON T. (2015)]

Emissive power and intensity

The radiative heat flux emitted from a body is called the emissive power. A distinction is made between total emissive power $e(T)$ and spectral or monochromatic emissive power $e_\lambda(\lambda, T)$.

$$e(T) = \int_0^\infty e_\lambda(\lambda, T)\, d\lambda \tag{2}$$

For a black body, the dependence of the emissive power on the temperature is expressed by the Stefan-Boltzmann law

$$e_b(T) = \sigma T^4 \tag{3}$$

where σ is the Stefan-Boltzmann constant, σ = 5.87 x 10^{-8} W/m²K⁴.

For grey bodies, the equation is similar but takes into account the emissivity ε of the material.

$$e_g(T) = \varepsilon\sigma T^4 \tag{4}$$

The intensity of radiation from a diffuse surface is uniform in all directions. For a black body, the intensity is the following:

$$I_b = \frac{e_b}{\pi} = \frac{\sigma T^4}{\pi} \tag{5}$$

Radiant heat exchange

For the case of an object k placed in an enclosed surface such as the area of the object is negligible when compared to the surrounding environment surface, the results can be simplified. The heat transferred by radiation from the object to the surrounding surface can then be calculated using this simple equation.

$$Q = A_k \sigma \varepsilon_k ({T_k}^4 - {T_{env}}^4) \tag{6}$$

The formula includes the surface area, emissivity and temperature of the object, the temperature of the surrounding environment and the Stefan-Boltzmann constant.

2.2. The equation of radiative transfer

The starting point for modelling heat transfer by radiation is the equation of radiative transfer. It describes the process of radiative transfer when incoming radiation of intensity I enters an absorbing, emitting, and scattering medium.

Attenuation

The incoming radiation loses some of its intensity through absorption and scattering in the medium. The losses are expressed as follows:

$$(dI)_{loss} = -(a + \mu_s)Ids \tag{7}$$

a is the absorption coefficient [m^{-1}] and μ_s the scattering coefficient [m^{-1}]. Sometimes in the literature another value can be found: the extinction coefficient $\beta = a + \mu_s$, also called opacity. ds is the distance travelled by the beam.

The optical thickness τ is a dimensionless quantity that characterizes the attenuation of optical radiation in the medium. It takes into account both absorption and scattering. The value combines the real thickness s, density ρ and opacity β of the material. If I_0 is the intensity emitted by a source and I is the intensity of this radiation at a given depth, the optical thickness τ is defined using the following formula.

$$\frac{I}{I_0} = e^{-\tau} = e^{-\beta\rho s} \tag{8}$$

Augmentation

As the medium is scattering and emitting, the incoming radiation is also augmented during its path through the medium. It receives the emission of the medium:

$$(dI)_{em} = aI_b ds \tag{9}$$

I_b is the black body intensity.

It also gains energy by scattering from other directions into the direction of travel. Since this augmentation has contributions from all directions, it must be calculated by integration over all solid angles. The resulting gain is:

$$(dI)_{sca}(\vec{s}) = ds\frac{\mu_s}{4\pi}\int_0^{4\pi} I(\vec{s}')\phi(\vec{s}', \vec{s})d\Omega' \tag{10}$$

$\vec{s}'$ is the scattering direction vector, ϕ the scattering phase function [sr^{-1}] and Ω' a solid angle [sr].

The equation of radiative transfer is a balance of the radiative energy based on the previous equations. In its quasi-steady form, at position $\vec{r}$ in direction $\vec{s}$, it is written as follows.

$$\frac{dI(\vec{r},\vec{s})}{ds} + (a+\mu_s)I(\vec{r},\vec{s}) = aI_b(\vec{r}) + \frac{\mu_s}{4\pi}\int_0^{4\pi} I(\vec{r},\vec{s}')\phi(\vec{s}',\vec{s})d\Omega' \qquad (11)$$

2.3. Radiation modelling in Fluent

For this study, the CFD software ANSYS Fluent was used. The following paragraphs are based on FLUENT (2006) documentation. The software provides five different models for heat radiation modelling to include radiation in heat transfer simulations: discrete transfer radiation model (DTRM), P-1 radiation model, Rosseland radiation model, surface-to-surface (S2S) radiation model, and discrete ordinates (DO) model.

2.3.1. Choosing a radiation model

The P-1 radiation model is the simplest case of the more general P-N model, which is based on the expansion of the radiation intensity I into an orthogonal series of spherical harmonics. The Rosseland model is the diffusion approximation for radiation derived from the P-1 model. It can be used only for optically thick media; its use is recommended when the optical thickness exceeds 3. The P-1 model can also lead to accuracy problem with optical thicknesses too low; it is typically used for optical thicknesses above 1. In this study, the medium which defines the optical thickness is air and the maximum length in the geometry of the problem is around 0.5 m. Therefore, this study operates at small optical thicknesses and the P-1 and Rosseland models cannot be used.

The S2S model considers only surface-to-surface radiation; it does not take into account any absorption, emission, or scattering of radiation between the surfaces. Therefore, it is only suitable for problems of radiative transfer with non-participating media, for example in applications, when the radiation exchange takes place in an enclosure of gray-diffuse surfaces.

In the case of this particular study, the S2S model would not be able to determine the radiative intensity in the space filled with air under the heater so it cannot be used.

The DTRM uses a "ray tracing" technique, assuming that the radiation leaving the surface element in a certain range of solid angles can be approximated by a single ray. This model does not allow specular reflection which will be needed at some point of the advancement of the project. Therefore, its use is not adequate in this study.

In light of the above discussion, the chosen model is the DO model of which the theory and use will be detailed in the following paragraphs.

2.3.2. The DO model

The discrete ordinates method uses a discrete representation of the directional variation of the radiative intensity, solving the equation of radiative transfer for a set of discrete directions. This method is actually a finite differencing of directional dependence of the equation of radiative transfer.

In Fluent, the DO model allows gray and non-gray radiation but only the gray radiation case will be discussed here. The non-gray case can be deducted using the same equations for the spectral intensity I_λ.

The DO model transforms the equation of radiative transfer into a transport equation for radiation intensity. For each direction $\vec{s}$, the model solves one transport equation with a solution method identical to that used for the fluid flow and energy equations. The equation (11) is transformed into a field equation and is therefore written as follows.

$$\nabla \cdot (I(\vec{r},\vec{s})\vec{s}) + (a+\sigma_s)I(\vec{r},\vec{s}) = aI_b(\vec{r}) + \frac{\mu_s}{4\pi}\int_0^{4\pi} I(\vec{r},\vec{s}')\phi(\vec{s}',\vec{s})d\Omega' \qquad (12)$$

Fluent uses a variation of the DO model called the **finite volume method**. It has the advantage to prevent the false scattering and ray effects that can occur with the DO method. Mainly its use is preferred because it ensures the conservation of radiative energy unlike the classic DO method. This method uses finite solid angle volumes instead of finite differences. Moreover, whereas the DO method replaces the integral the equation (11) by numerical quadratures, the

finite volume method uses exact integration to evaluate the solid angles integrals. It gives a fully finite volume approach, in space as well as in direction.

There are two implementations available for the DO model in Fluent: uncoupled and energy coupled. The uncoupled one solves the equations for energy and radiation intensities one by one. In the coupled approach, the discrete energy and intensity equations are solved simultaneously at each cell. The main advantage is that it speeds up the simulation for certain cases involving high optical thicknesses or scattering coefficients.

2.3.2.1. Angular discretization

In Fluent, the angular discretization is controlled by the user by means of the angles θ and ϕ. They are the polar (zenith) and azimuthal angles respectively, defined as showed in Figure 2. Each control angle is associated with a direction $\vec{s}$ characterized by the two control angles. The user can choose the number of divisions associated to each angle: each octant of the angular space 4π is discretized into the chosen number of divisions for θ and ϕ. For a 2-D case, it is possible to align the case plan to the (x,y) or (y,z) plan so that θ or ϕ respectively become irrelevant.

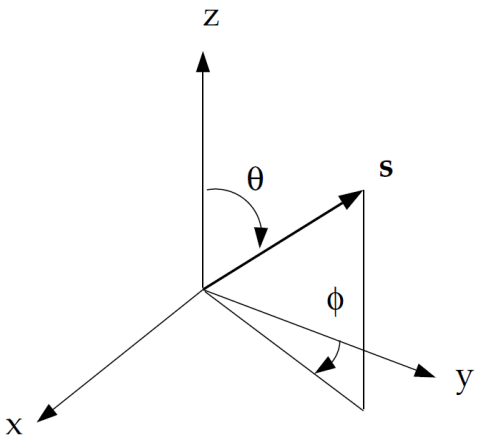

FIGURE 2. ANGULAR COORDINATE SYSTEM FOR THE DO MODEL [FLUENT (2006)]

As control volume faces do not in general align with global angular discretization, it can lead to the problem of control angle overhang: control angles being partially incoming and partially outgoing to the face. The correction of this problem is done using pixelation. Each control angle is divided into a certain number of pixels as depicted in Figure 3. The energy contained in each pixel is then treated as incoming or outgoing to the face. As well as the number of divisions, the number of pixels is chosen by the user.

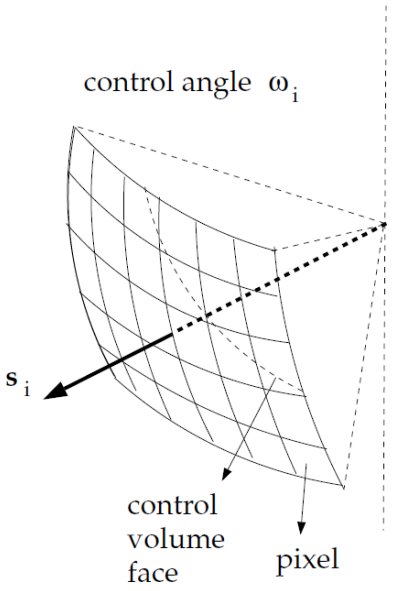

FIGURE 3. PIXELATION OF A CONTROL ANGLE [FLUENT (2006)]

2.3.2.2. Boundary conditions

The Fluent DO model allows the specification of opaque and semi-transparent walls. However, only opaque walls are needed in this study thus only their boundary conditions will be describe below.

When incident radiation arrives on an opaque wall, a part of it is reflected, both diffusely and specularly, depending on the diffuse fraction of the wall f_d and the reflectivity (which is directly related to the emissivity because of the opacity of the wall). The other part of the incident radiation is absorbed and the wall also emits some radiation. The quantity of both absorbed and emitted radiation are dependent on the emissivity of the wall ε_w. Since the wall is opaque, no radiation is transmitted through it. This process is illustrated on Figure 4.

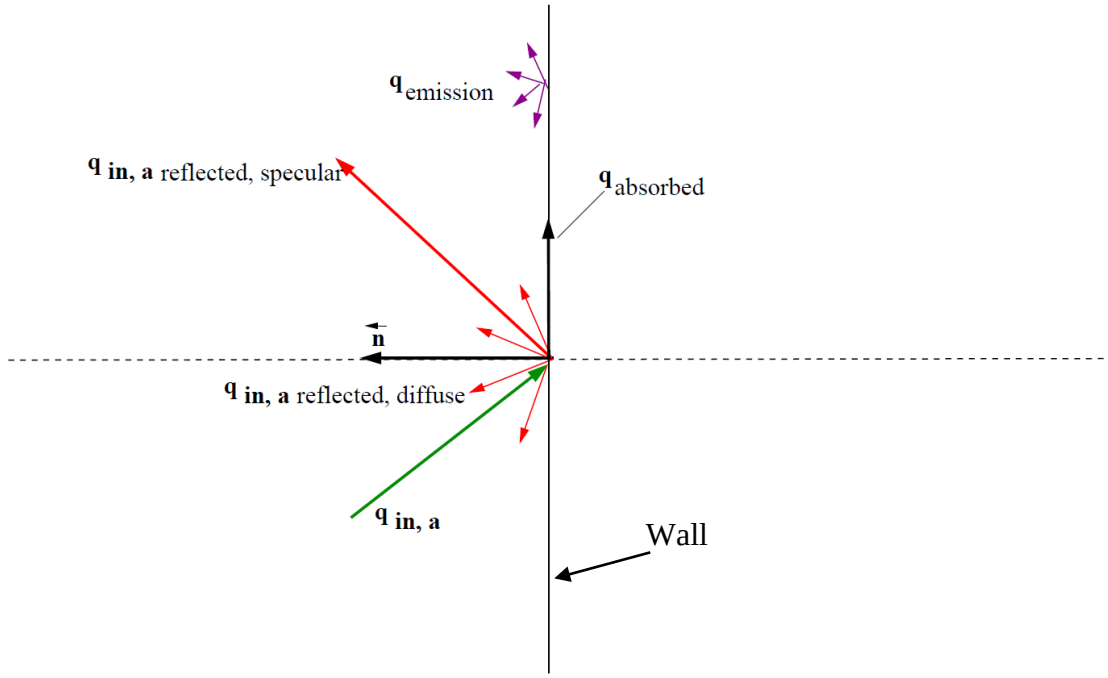

FIGURE 4. RADIATION ON AN OPAQUE WALL (BASED ON FLUENT [2006])

The medium "a" is an adjacent fluid or solid.

If the quantity of radiative energy incident on the opaque wall is written q_{in}, the different amounts of diffused, emitted and absorbed radiation are:

- Diffusely reflected energy = $f_d(1-\varepsilon_w)q_{in}$
- Specularly reflected energy = $(1-f_d)(1-\varepsilon_w)q_{in}$
- Energy absorbed at the wall surface = $\varepsilon_w q_{in}$
- Energy emitted from the wall surface = $\varepsilon_w \frac{I_b}{\pi}$, where I_b is the black body radiation intensity.

For diffuse walls, the boundary condition at the wall for the radiative intensity is as follows.

$$I(\overrightarrow{r_w},\vec{s}) = \varepsilon_w I_b(\overrightarrow{r_w}) + \frac{1-\varepsilon_w}{\pi}\int_{\vec{n}.\vec{s'}<0} I_{in}\left(\overrightarrow{r_w},\overrightarrow{s'}\right)\left|\vec{n}.\overrightarrow{s'}\right| d\Omega' \qquad (13)$$

For specular walls, if the interface normal is written $\vec{n}$ and the incident direction $\vec{s}$, the direction of the reflected ray $\overrightarrow{s_r}$ is given by the following equation.

$$\overrightarrow{s_r} = \vec{s} - 2(\vec{s}.\vec{n})\vec{n} \qquad (14)$$

3. Preliminary tests

The first step in this study is to run some preliminary tests on the DO model in Fluent. These tests will determine the setup to use for all the simulations on the real geometry.

For all following tests, ANSYS Workbench was used to create geometries and meshes, and Fluent was used for the simulations.

3.1. General considerations

There are several parameters that have to be tested and then fixed. The first ones concern the angle discretization in the DO model; for θ and ϕ divisions and pixels, some values must be chosen. The density of the numerical mesh must also be fixed; an optimum between too coarse and too fine must be found. Finally, the splitting of the surfaces is also considered and tested to see if it influences the results in any way.

The tests were performed using two different geometries, simpler than the ones that were used later for the core of the study. As the real geometry is represented in two dimensions, all of the preliminary tests are also in 2-D. The first geometry used is a simple tube of 100 mm diameter (represented by a circle in 2-D) in the middle of a square which stands for the ambient environment. Each side of the square measures 500 mm. The second geometry is a semi-circle of 500 mm radius, with a 10 mm heated line in the middle of its bottom part. Again the semi-circle and the bottom part around the heated element stand for the environment.

For the DO model, the uncoupled implementation was used.

For all the tests, all the surfaces were taken as diffuse (diffuse fraction of 1) with an internal emissivity of 1. Regarding the temperature, for the first series of tests, the environment temperature was taken as 25 °C (298.15 K) and the tube temperature as 350 °C (623.15 K). For the tests using the second geometry, a higher temperature difference was tried and therefore the environment temperature was fixed at 200 K and the heated element temperature at 600 K.

During all the testing a uniform mesh was used, meaning that the growth rate of mesh elements was fixed at 1. This choice was made because the aim of the simulations is to visualize what is happening in the whole simulation domain. There is no zone of the geometry for which the meshing can be coarser.

3.2. First geometry: tube in a square

The first set of tests was performed using the geometry showed on Figure 5, described in the previous part. In these tests, the observed results were the graphical representation of the incident radiation in the simulation domain. The objective of the optimization of the variables was to obtain smooth isolines of incident radiation. This preliminary study was performed in three phases: angle discretization, mesh size and surface splitting. Combining these parameters was also tried.

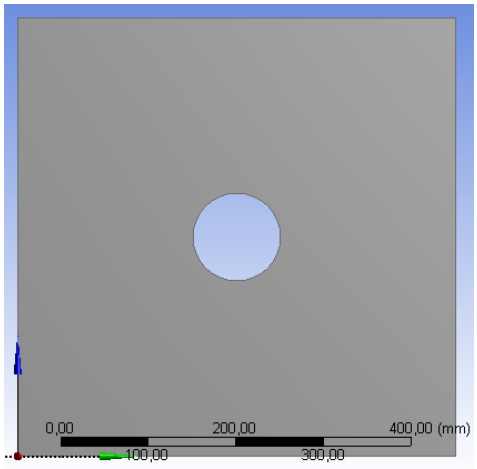

FIGURE 5. FIRST SIMPLIFIED GEOMETRY

3.2.1. Angle discretization

For θ and ϕ divisions and pixels, the best values to choose have to be determined. First each parameter is tested separately to try and find its optimal value. Only one parameter is changed at a time while all the others are kept at their default values. Then it is hoped than by combining the optimal values will give a good result. For these tests, a triangular mesh with triangles of 8 mm side was used, arbitrarily chosen because the optimal mesh size was not known yet.

The analysis begins with the examination of the angle θ. Actually, because the geometry is in 2-D and represented in the (x,y) plan, as explained in the previous chapter, this angle should be irrelevant. Neither its divisions nor pixels should have an influence on the results. This was actually proved by these simulations. It was observed that increasing θ divisions does not change the results and that the same goes for θ pixels. Therefore, only the angle ϕ is relevant for this study's problem.

The default value for ϕ divisions is 2. Increasing this value has an influence on the results but also on the simulation time which is longer. Different values of divisions were tried, all values from the default one to 18. The obtained results are displayed on Figures 6 to 11. The best results were obtained with 15 divisions.

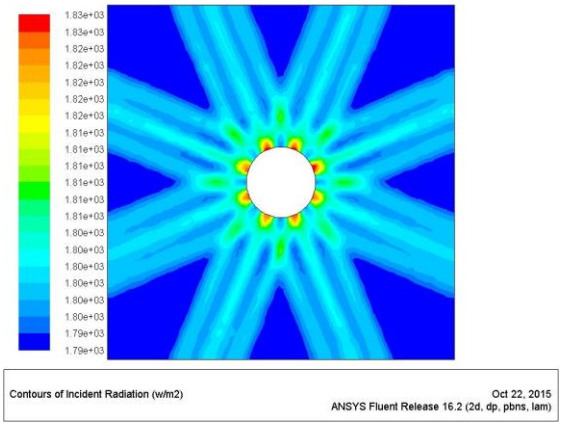

FIGURE 6. ϕ DIVISIONS = 2

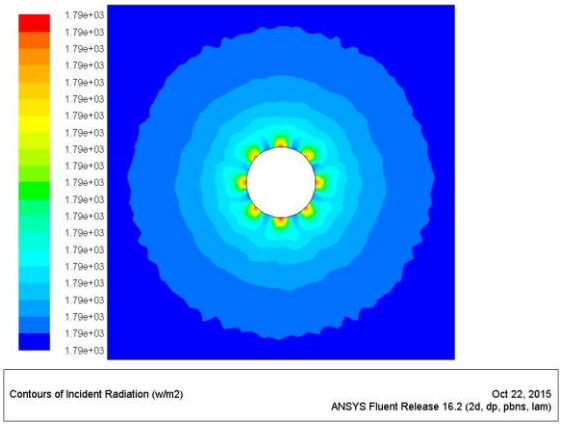

FIGURE 9. ϕ DIVISIONS = 12

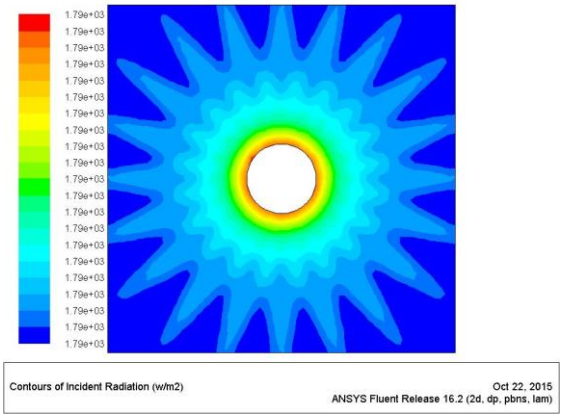

FIGURE 7. ϕ DIVISIONS = 5

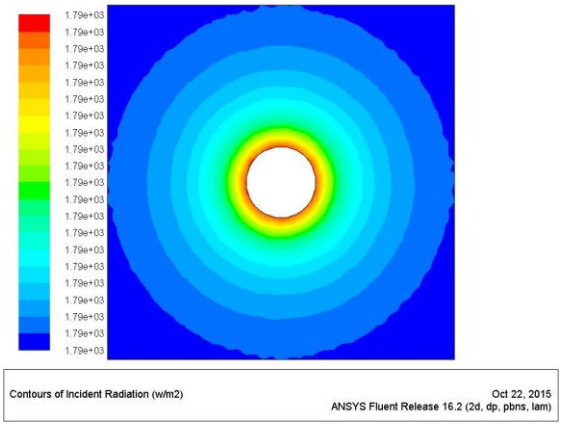

FIGURE 10. ϕ DIVISIONS = 15

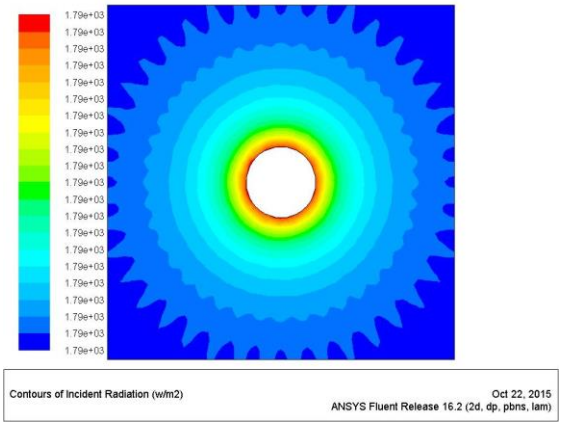

FIGURE 8. ϕ DIVISIONS = 10

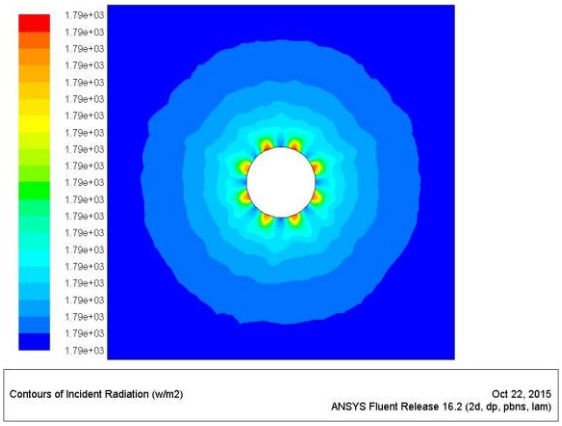

FIGURE 11. ϕ DIVISIONS = 18

The images (Figure 6 to Figure 11) illustrate the significance of angle divisions. The number of peaks of radiation observed on the pictures is directly related to the number of divisions chosen. As described in the previous chapter, choosing for example 5 ϕ divisions gives a partition of each quadrant of the simulation surface in 5 control angles. On the pictures, it can be seen that in this configuration, in each quadrant there are 5 peaks of radiation.

The same procedure was done for ϕ pixels and results are displayed on Figure 12 to 15. The number of pixels was increased from the default value 1 to 11, while the number of divisions is kept at the default value (= 2). It was noticed that increasing the number of pixels slows down the computation but not as much as increasing the number of divisions. It can also be observed that changing the pixelation has less influence on the results than changing the number of divisions: alone it cannot give smooth lines of incident radiation like seen previously with the ϕ divisions. The best results found here could be with 5 pixels.

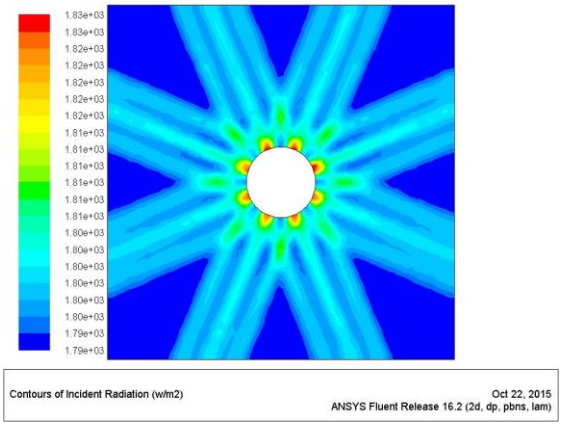

FIGURE 12. ϕ PIXELS = 1

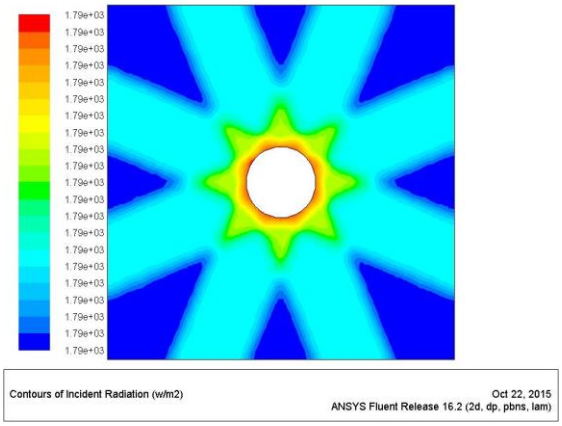

FIGURE 14. ϕ PIXELS = 5

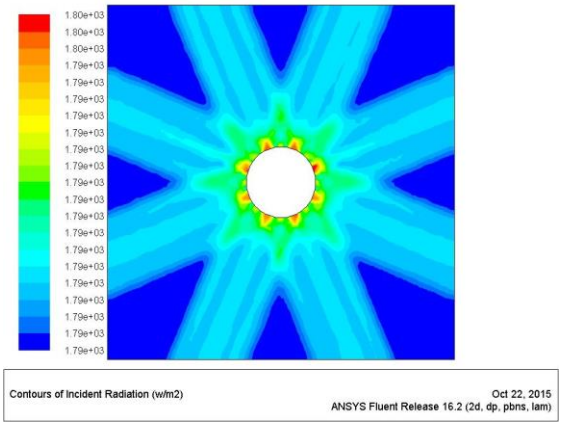

FIGURE 13. ϕ PIXELS = 3

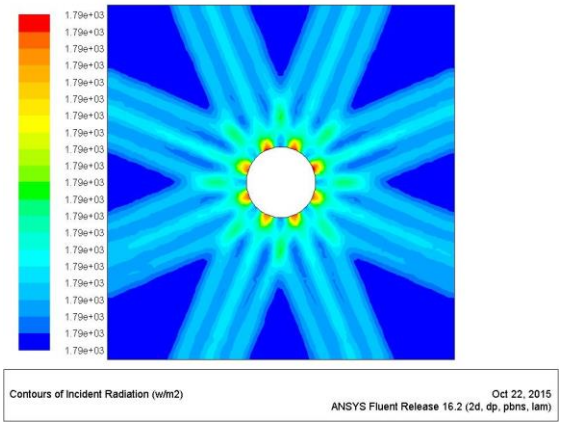

FIGURE 15. ϕ PIXELS = 11

Unfortunately, combining the two optimal values found for ϕ divisions and pixels did not give a satisfying result (Figure 16). The lines were not smooth but rather scattered further away from the tube. Therefore, some other couples (divisions; pixels) of values were tried but the smoothest lines were obtained by the combination (15;1) and pictured on Figure 10. Very similar results are acquired with the combination (15;2) and depicted on Figure 17.

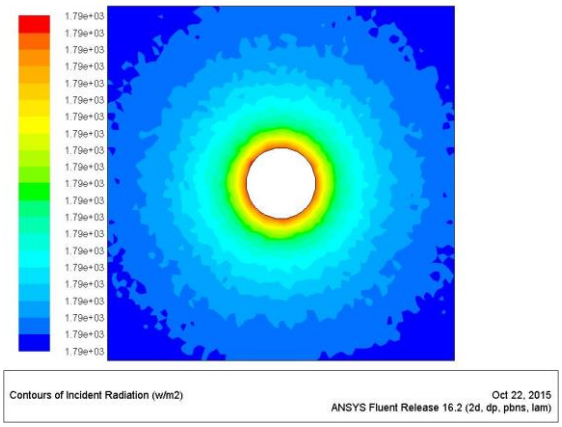

FIGURE 16. RESULTS FOR (15;5)

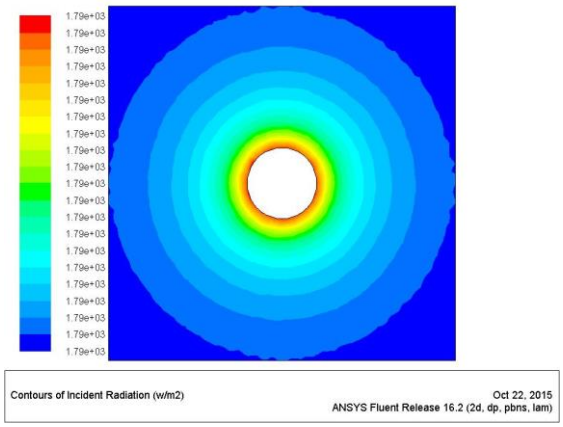

FIGURE 17. RESULTS FOR (15;2)

3.2.2. Size of the mesh

This part of the study was done to ensure that the results would only be changing with boundary conditions and not with mesh conditions. It is called a grid sensitivity study and consists in finding the mesh size from which the results vary only slightly with a change in the mesh. Using the default values for the discretization angles, different meshing is tested.

Here, only a triangular uniform mesh is considered. The only difference between the meshes is the size of the side of the triangles. The first tests, described in the previous part, were done with a mesh of 8 mm triangles i.e. 7 716 elements. Coarser and finer meshes were tested here, from 10 mm triangles (5 138 elements) to 3 mm triangles (56 201 elements). The radiation contours are compared, as in the previous tests, and the minimum and maximum incident radiation are also studied.

The problem that was encountered is that the results kept changing with the size of the mesh. When the mesh became finer, the radiation contours appeared sharper, as showed on Figures 18 to 21.

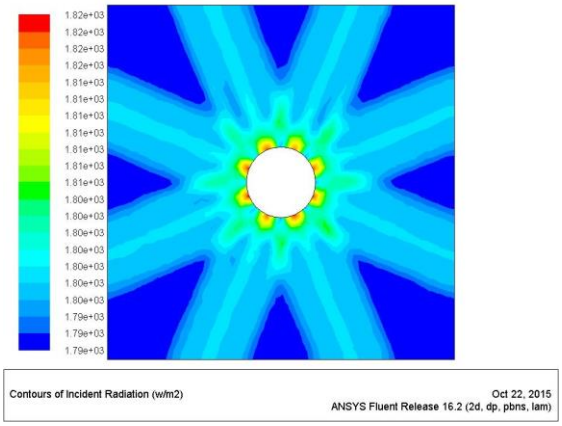

FIGURE 18. 10 MM TRIANGLES

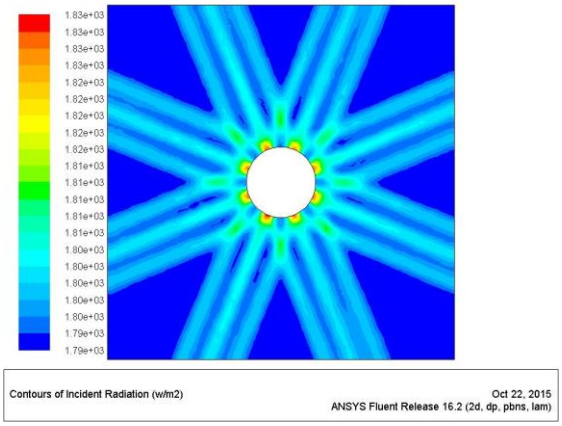

FIGURE 20. 6 MM TRIANGLES

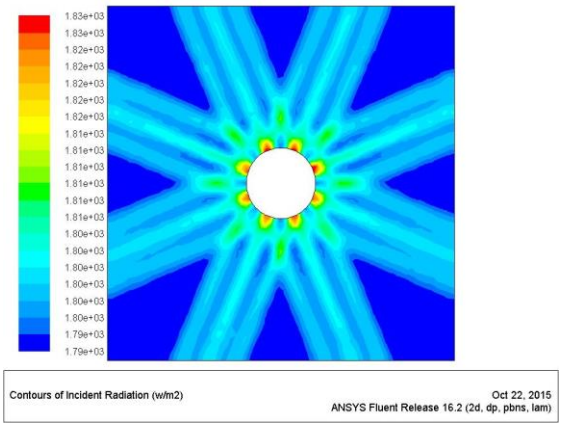

FIGURE 19. 8 MM TRIANGLES

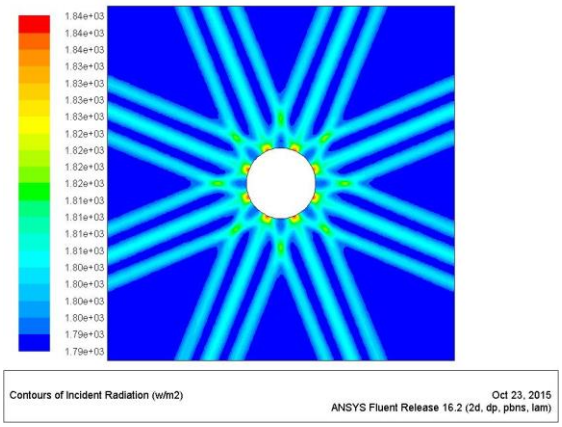

FIGURE 21. 3 MM TRIANGLES

Concerning the incident radiation values, the minimum never changed with the mesh size. The maximum incident radiation however increased when the mesh became finer as can be seen in Table 1.

TABLE 1. MAXIMUM RADIATION FOR DIFFERENT MESH SIZES

Mesh size (mm) (triangle side)	10	8	7	6	5	4	3
Maximum radiation (W/m²)	1 820.6	1 828.3	1 828.1	1 834	1 834	1 837.4	1 839.9

In the simplified geometry used in this preliminary study and in the one of the real radiant heater, the tubes have a diameter around 100 mm. Thus the perimeter is around 300 mm. If an 8 mm triangular mesh is chosen as in the angular discretization study, only about 35 triangles would be around the tube which is not enough to properly model the problem. That is why some

additional tests were performed to study more thoroughly meshes of 4, 5 and 6 mm triangles (respectively 31 685, 20 343, 13 875 elements). In these supplementary tests, various angular discretizations were examined, from 10 divisions up to 24. Changing the size of the mesh changes also the conclusions on angle discretization. Generally it is noticed that finer is the mesh, greater must be the angle discretization. This concerns especially the number of divisions. If for 8 mm triangles mesh, satisfying results had been found with 15 divisions, for 5 mm triangles mesh for example, the number of divisions must be increased up to around 20. Even then, the incident radiation lines appear to be smooth farther away from the tube but not in its immediate vicinity where they have a pattern similar to a flower. Additionally, some strange results appear for certain couple of values that are difficult to explain. Some of the results obtained are displayed on Figures 22 to 29.

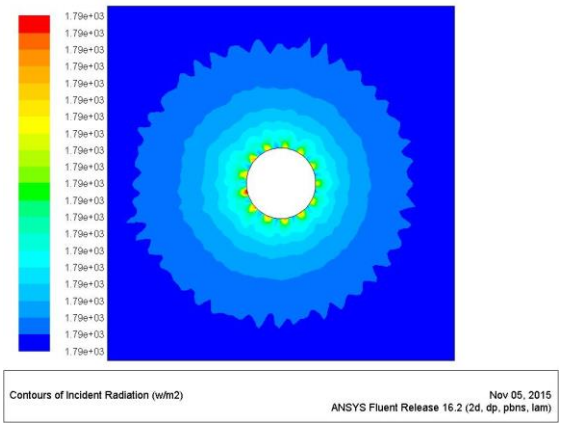

FIGURE 22. 6MM MESH - 10 DIVISIONS / 1 PIXEL

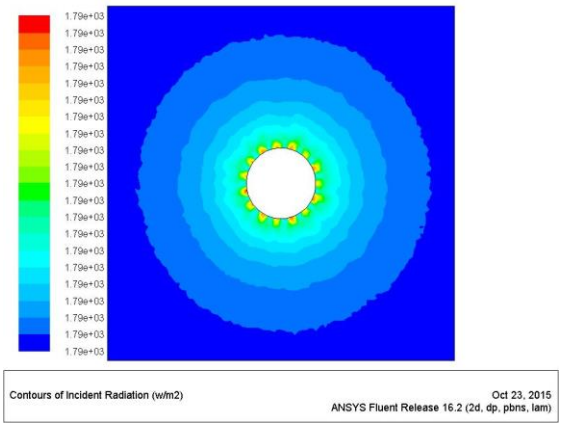

FIGURE 24. 6MM MESH - 18 DIVISIONS / 2 PIXELS

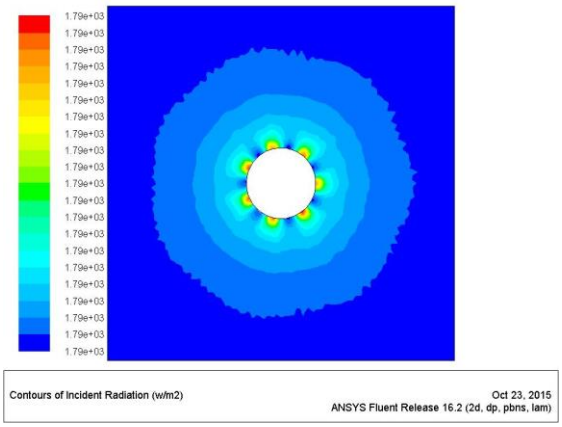

FIGURE 23. 6MM MESH - 15 DIVISIONS / 1 PIXEL

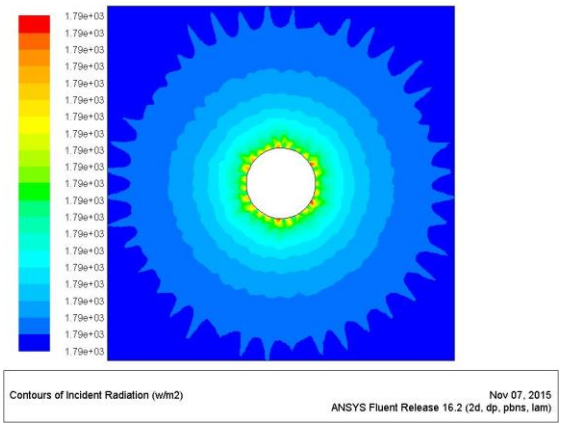

FIGURE 25. 5MM MESH - 10 DIVISIONS / 1 PIXEL

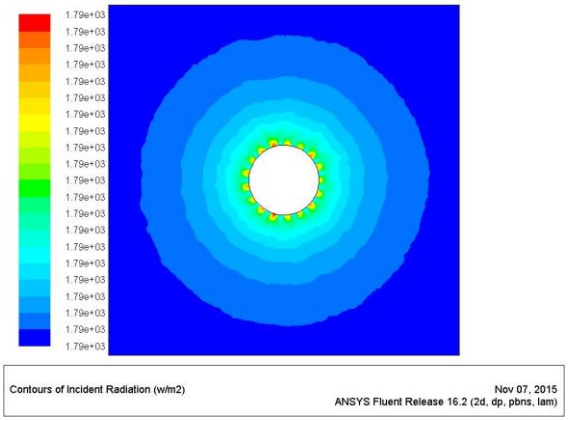

FIGURE 26. 5MM MESH - 20 DIVISIONS / 1 PIXEL

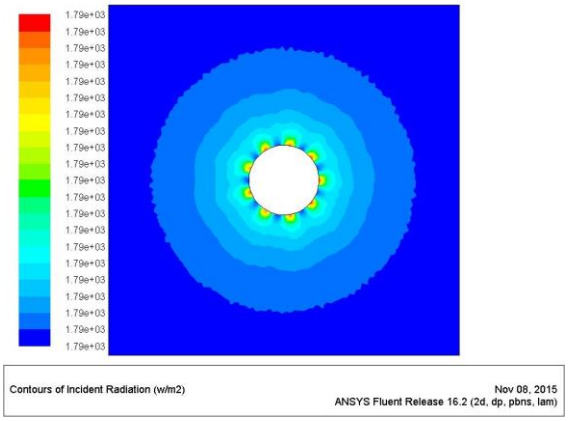

FIGURE 28. 4MM MESH - 18 DIVISIONS / 1 PIXEL

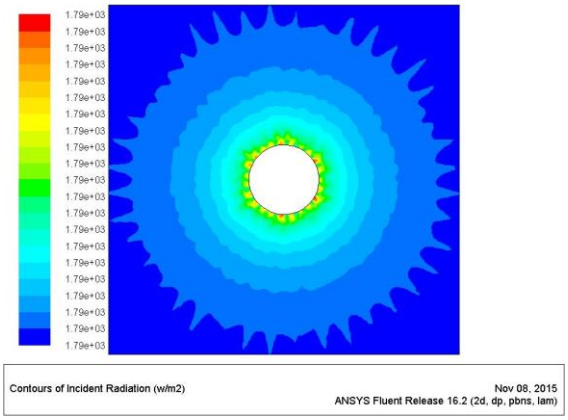

FIGURE 27. 4MM MESH - 10 DIVISIONS / 1 PIXEL

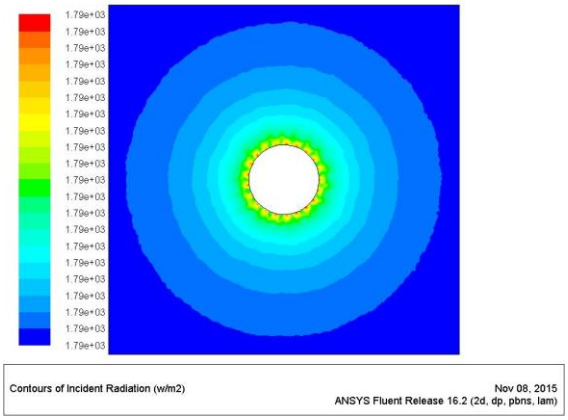

FIGURE 29. 4MM MESH - 21 DIVISIONS / 1 PIXEL

3.2.3. Surface splitting

Surface splitting was tried because it can improve the results sometimes. It was applied first to the tube and then to the square that stands for the environment. The tube was equally divided into 4, then 8 sections. For the square, each side was divided in 2, then 4 sections. Using a 5 mm triangular mesh, different angle discretizations were tried (couple (divisions; pixels)).

The results obtained are displayed in Figures 30 to 35. For the tube segmentation, the first splitting (into 4 sections) did have an influence but not in a significant way: the results obtained were only very slightly different than the ones without splitting. Then, splitting again each section in 2 did not change the results anymore. For 4 or 8 tube sections, the results were identical.

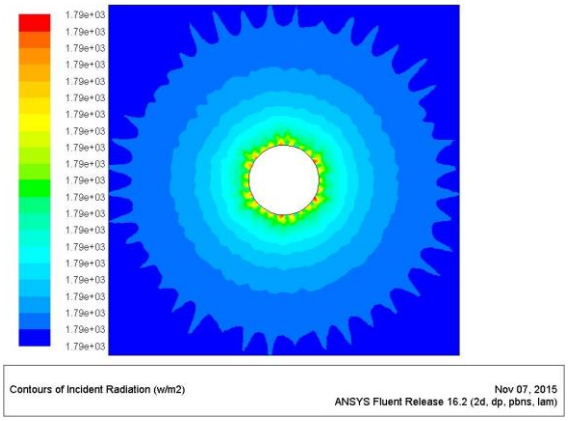

FIGURE 30. NO TUBE SPLITTING – ANGLE (10;1)

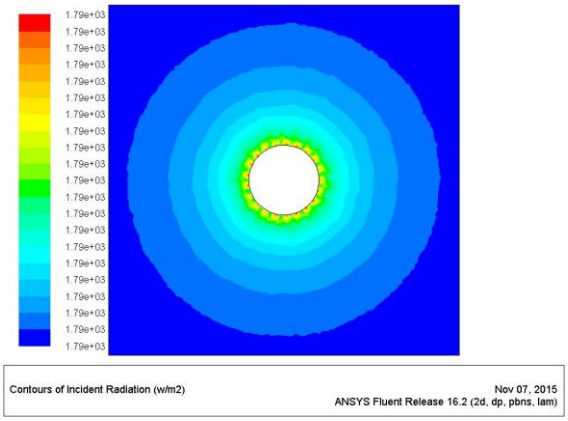

FIGURE 33. NO TUBE SPLITTING – ANGLE (21;1)

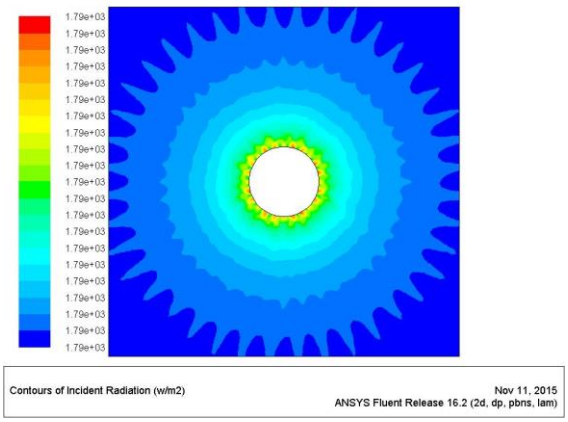

FIGURE 31. 4 SECTIONS – ANGLE (10;1)

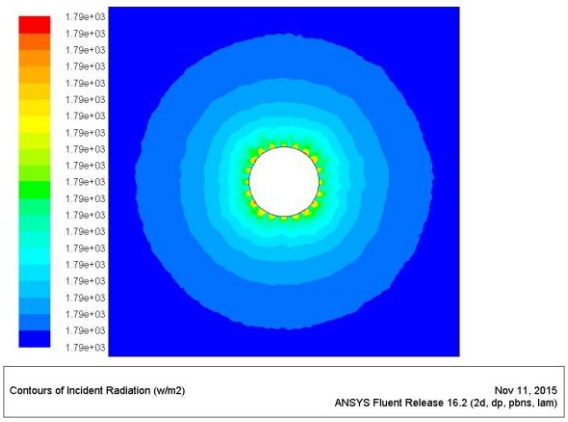

FIGURE 34. 4 SECTIONS – ANGLE (21;1)

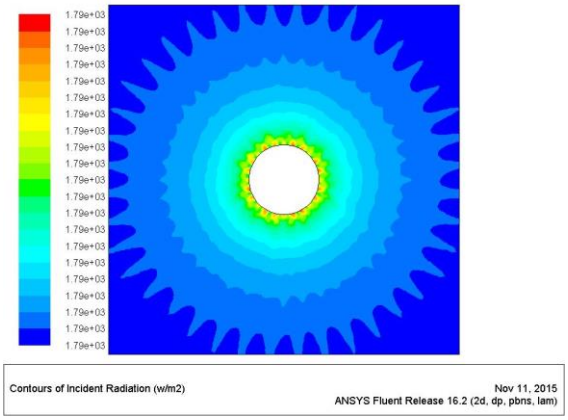

FIGURE 32. 8 SECTIONS – ANGLE (10;1)

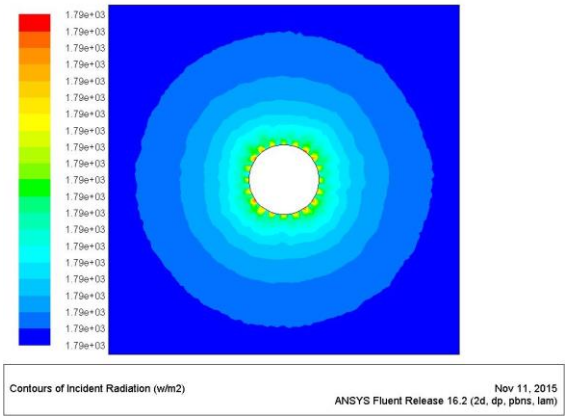

FIGURE 35. 8 SECTIONS – ANGLE (21;1)

Concerning the segmentation of the environment, the results obtained were identical whether it was without splitting, with 2 sections or 4 sections.

The small differences observed on the pictures can be only be a change in the display of the results, since the mesh is aligned differently around the tube and thus in the whole domain when the tube is split. Therefore, the results could be exactly the same but only appearing different when displayed on the picture. Moreover, it must be kept in mind that the graphs produced by Fluent are made by interpolation of real results. They do not show the exact reality of the results. In conclusion here it can be said that splitting surfaces does not influence the results and is useless for this study.

3.3. Second geometry: semi-circle

Since the previous set of tests were not suitable to conclude on the set up to use for the study, a second one is done using a different geometry. This time, a higher temperature difference is used and, from the results of the previous tests, a smaller range of configurations is tested. The study is done with meshes of triangles and of quadrilateres, of 10 mm, 5 mm and 2 mm side. Concerning the angle discretization, it is done with 4, 10, 15 and 18 ϕ divisions and 1, 3 and 5 ϕ pixels.

For this part of the study, the evaluation of the results is changed. Here, an evaluation line is incorporated in the geometry: a semi-circle of 0.3 m radius inside the evaluation surface, as can be seen on Figure 36. The solution data of incident radiation were exported on this line from Fluent into Excel. Then, the coordinates *(x,y)* are converted in one coordinate *s* representing the arc length from the point A.

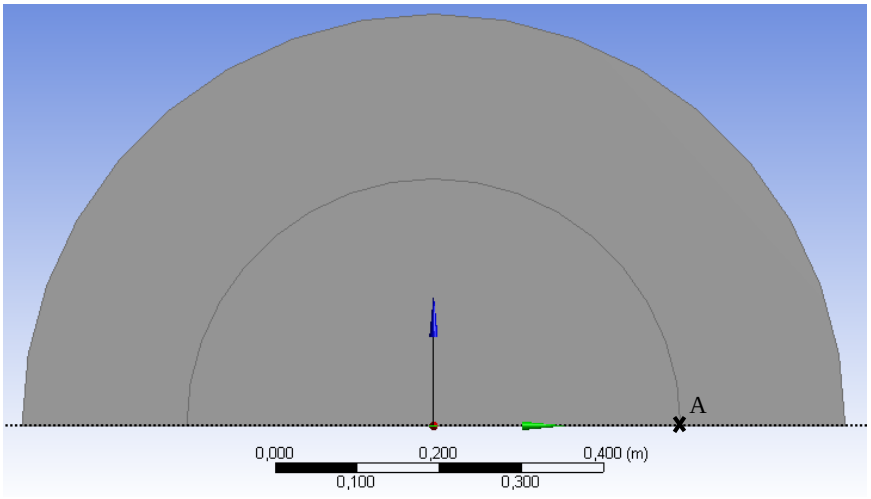

FIGURE 36. SECOND SIMPLIFIED GEOMETRY

The incident radiation is displayed in function of this new coordinate. The results obtained are described in the following graphs on Figures 37, 38 and 39.

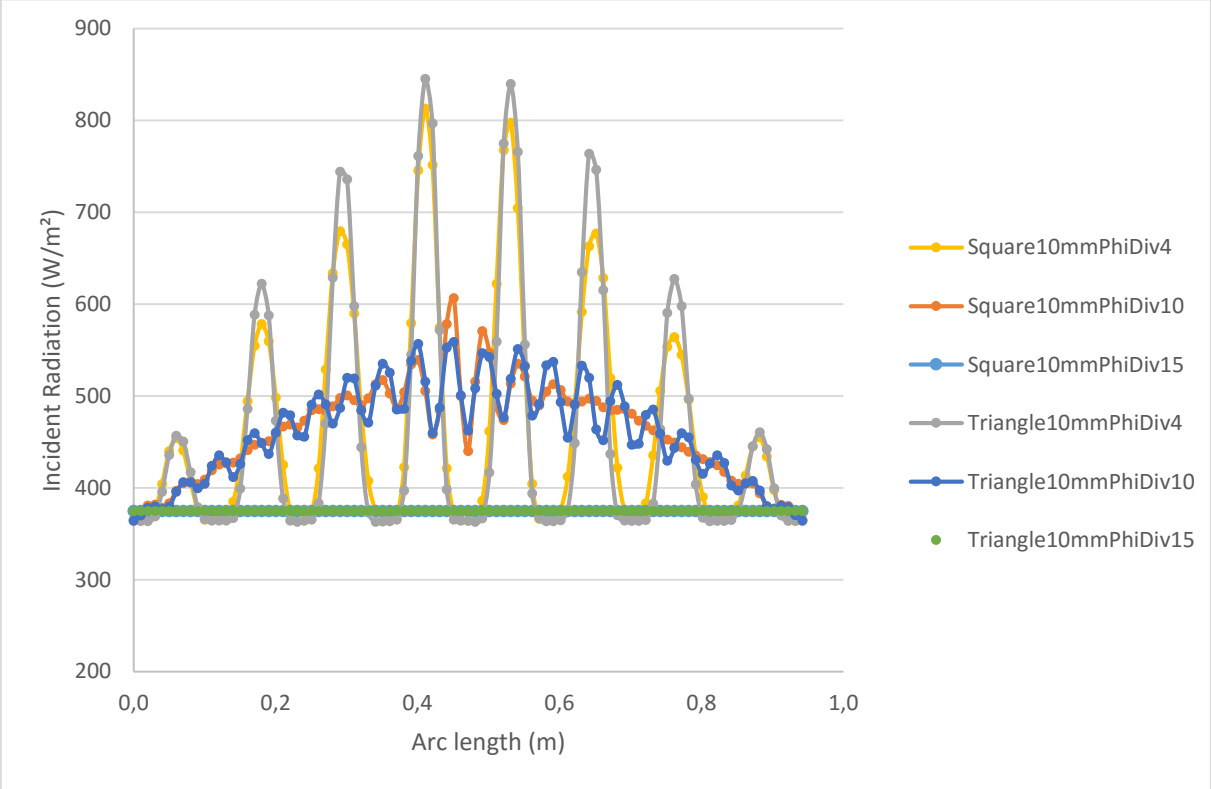

FIGURE 37. INCIDENT RADIATION FOR 10 MM MESHES

As it could be expected, the results for 4 ϕ divisions are not satisfying: really far from the other results and oscillating. The results for 10 ϕ divisions and 1 ϕ pixel are not really good either.

It can also be noticed that a triangular mesh of a given side size gives almost the same results than a quadrilateral mesh of the same side size. As triangular meshes have more elements than quadrilateral ones, the computation time induced is longer for meshes of the same side size. Therefore, if the results are equivalent, it can be concluded that it is better to use a quadrilateral mesh.

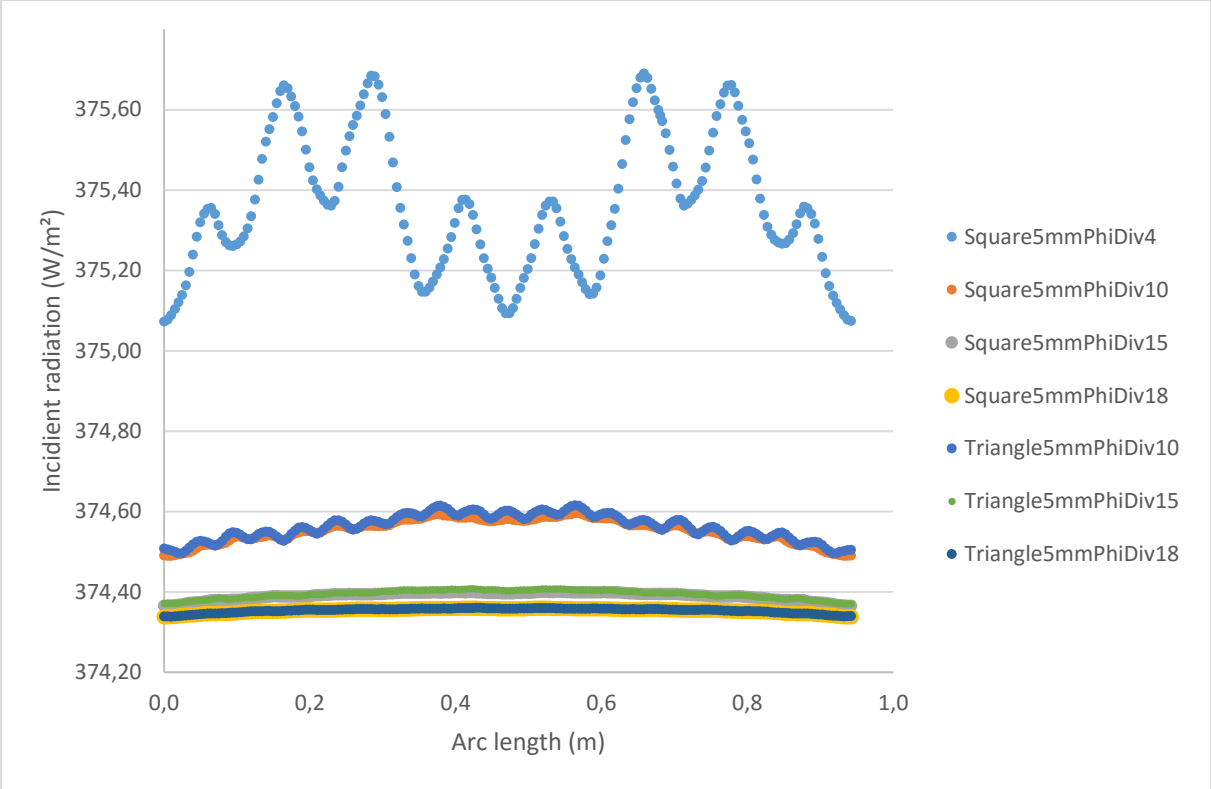

FIGURE 38. INCIDENT RADIATION FOR 5 MM MESHES

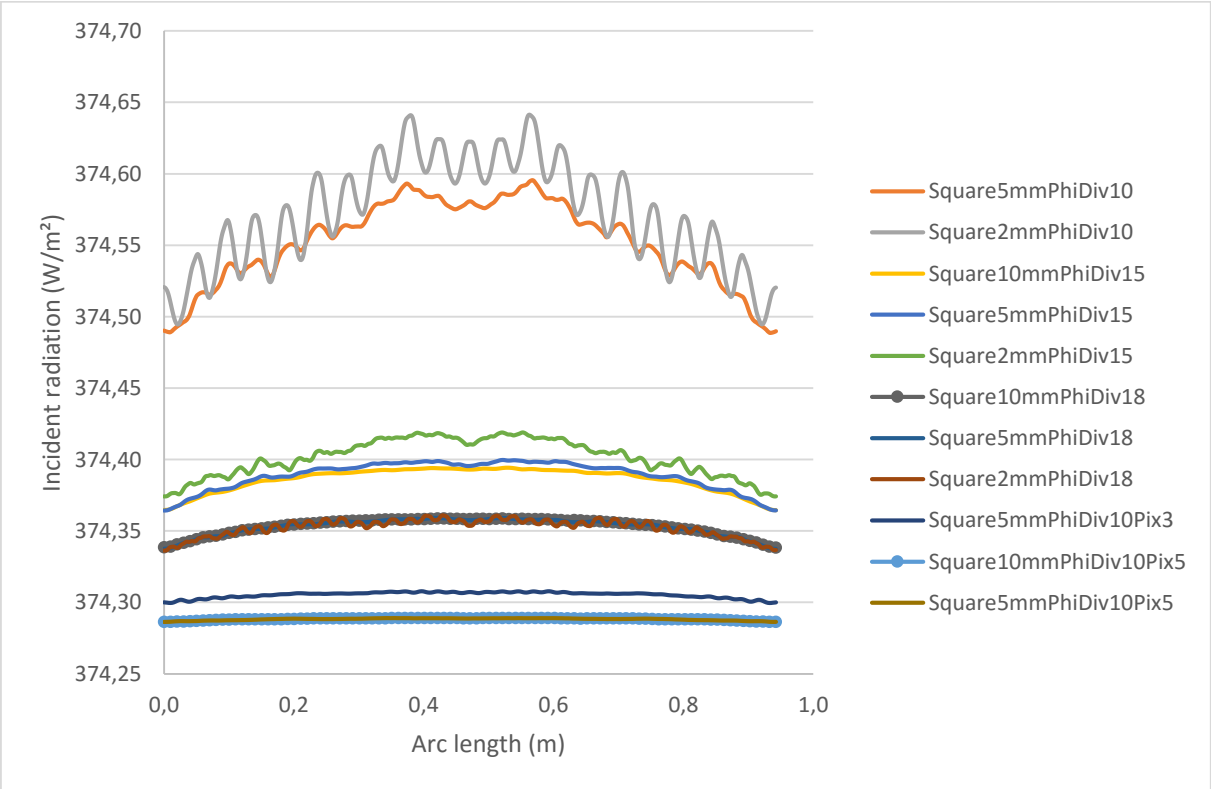

FIGURE 39. OVERVIEW FOR DIFFERENT CONFIGURATIONS

Regarding the computation time, the worst thing to do is to increase the mesh density (number of control volumes). It is better to increase the number of divisions and even better to increase only the number of pixels. It can be seen that, even though 10 divisions alone do not give good results, increasing the number of pixels improve the results.

Here, refining the mesh from 5 mm squares to 2 mm squares does not seem to influence the results. Therefore, we can conclude that keeping a 5 mm mesh is enough.

It can also be noticed that all the results are more or less curved whereas perfectly constant incident radiation can be expected for this problem (emitting element in the center of the semi-circle). This could be explained by the fact that the two parts of the "bottom" boundary around the heated element also emit some radiation, even though it is less than said element. It can influence the results in the observed way.

The best configuration here seems to be a 5 mm square mesh with 10 ϕ divisions and 5 ϕ pixels. 18 ϕ divisions and 10 ϕ divisions with 3 pixels seem to be also acceptable.

It is reminded here that all the simulations in this chapter used the uncoupled implantation of DO radiation model and energy. It will be seen in the next chapter that it can actually explain some strangeness of the results obtained. For example, the radiation here only varied in a very small range in the pictures showed and some unexpected phenomena in the shape of radiation were observed. Changing to the coupled implementation would probably fix these problems but it was not known at that time.

4. Tube radiant heaters

4.1. General information

Radiative heat transfer is used in the heating industry via two basic types of radiant heaters: luminous and tube radiant heaters. It is the latter that is interesting in regard of this study.

Radiant heaters are a form of decentralized heating meaning that, contrary to central heating, the heat is produced at the place where it is wanted and there is no need to transport the energy. They are especially suitable to heat large spaces like warehouses, hangars… This heating system is very efficient as heat radiation travels through air with almost no loss and heats only when hitting surfaces which will also radiate heat back in the environment.

Plus, in radiant heaters, since they are a decentralized heating system, no energy is lost during transport contrary to central heating which increase the efficiency. Another advantage is that the heating time is generally really short for this type of heating system.

Radiant tube heaters are gas-fired infrared heating devices. They use infrared radiation to produce heat. A gas burner generates a long laminar flame inside the tube. Generally, the tube diameter is around 100 mm but can go up to 400 mm for special types. The surface of the tube is then heated up to a temperature typically between 200 and 600 °C and thus emits heat radiation. An exhaust gas system is there to discharge the gasses released by the combustion into the atmosphere. A reflector is placed above the tube and designed so that the heat radiation is directed to the occupancy area. Insulation can be added to reduce the heat loss through the reflector. A diagram of a tube radiant heater is presented on Figure 40.

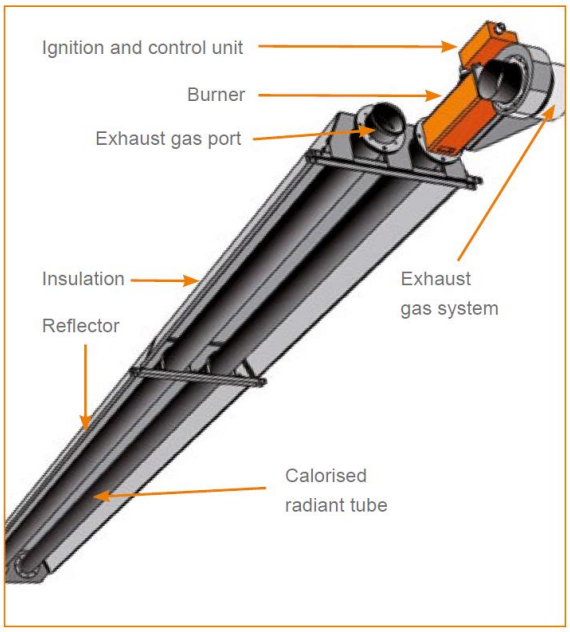

FIGURE 40. DIAGRAM OF A TUBE RADIANT HEATER [SCHWANK (2015)]

Tube radiant heaters can be in L-shape or in U-shape as illustrated in Figure 41. In this study, only U-shape radiant heaters are used.

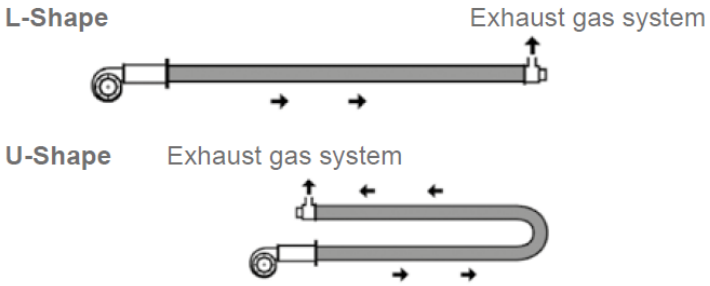

FIGURE 41. L-SHAPE AND U-SHAPE OF TUBE RADIANT HEATERS [SCHWANK (2015)]

4.2. Different geometries used

In this study, seven different geometries of real tube radiant heaters are compared. They are taken from various manufacturers and of various types.

The first geometry used is the one used for the set up tests: Kotrbatý KM. Some similar geometries with only one reflector above the two parts of the tube are studied: Mandík Helios 50, Schwank calorSchwank 50U, Schwank calor Schwank LL and Carlieuklima MSC9. In

addition, two heaters with separated reflectors are also examined: Carlieuklima MSU9 and Pakole Zenit 12. These geometries were taken from contents available on-line ([Kotrbatý], [Mandík], [Carlieuklima], [Schwank], [Pakole]).

To be able to compare their performances, all the heaters are taken with tubes of the same diameter 102 mm. In this way, the results will only be dependent on the reflector shape and the comparison will be possible. Only two heaters are modified: Mandík Helios 50 and Pakole Zenit 12 which have in reality tubes of 108 mm diameter.

The geometries used are showed on Figures 42 to 48.

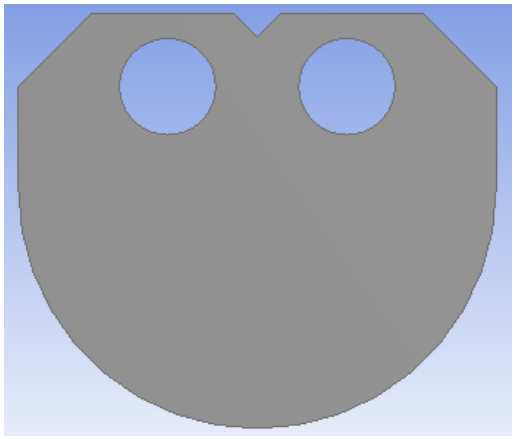

FIGURE 42. KOTRBATÝ KM

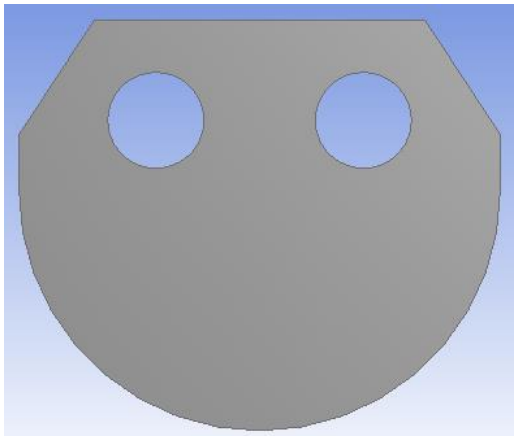

FIGURE 43. MANDÍK HELIOS 50

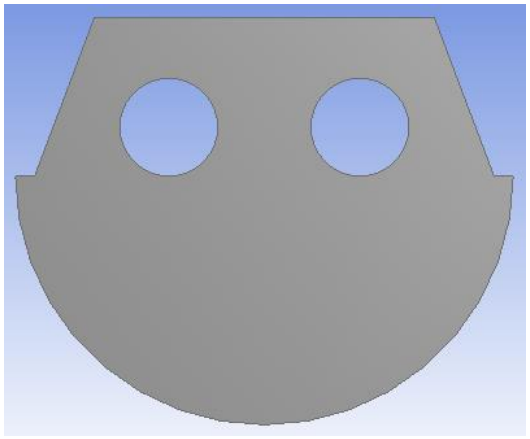

FIGURE 44. SCHWANK CALORSCHWANK 50U

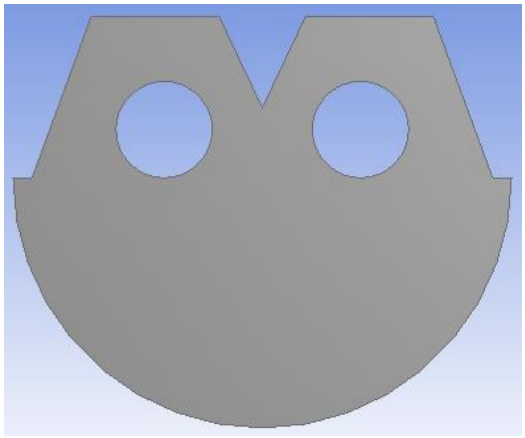

FIGURE 45. SCHWANK CALORSCHWANK LL

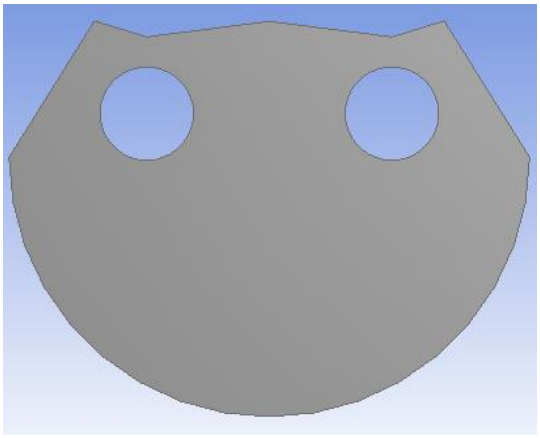

FIGURE 46. CARLIEUKLIMA MSC9

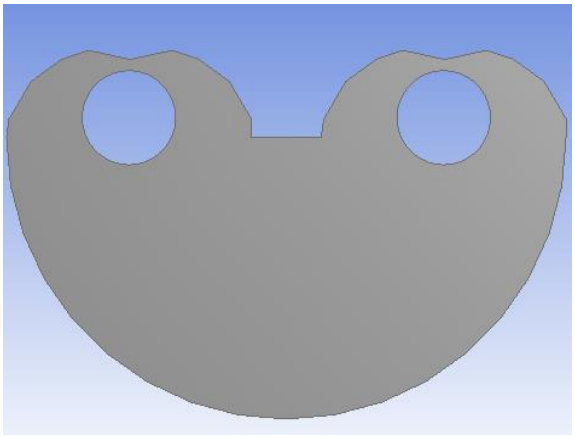

FIGURE 48. PALOLE ZENIT 12

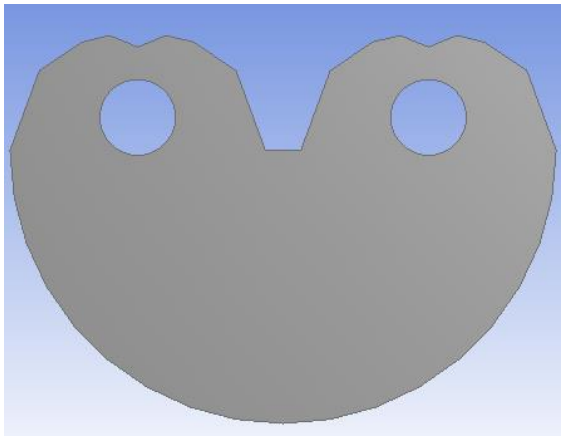

FIGURE 47. CARLIEUKLIMA MSU9

5. Set up tests with real geometry

After using simpler geometries, the first real geometry of a tube radiant heater was used to perform some additional set up tests. The best configurations found in the precedent chapter were applied to it. The geometry used is the one of the heater KM from the manufacturer Kotrbatý.

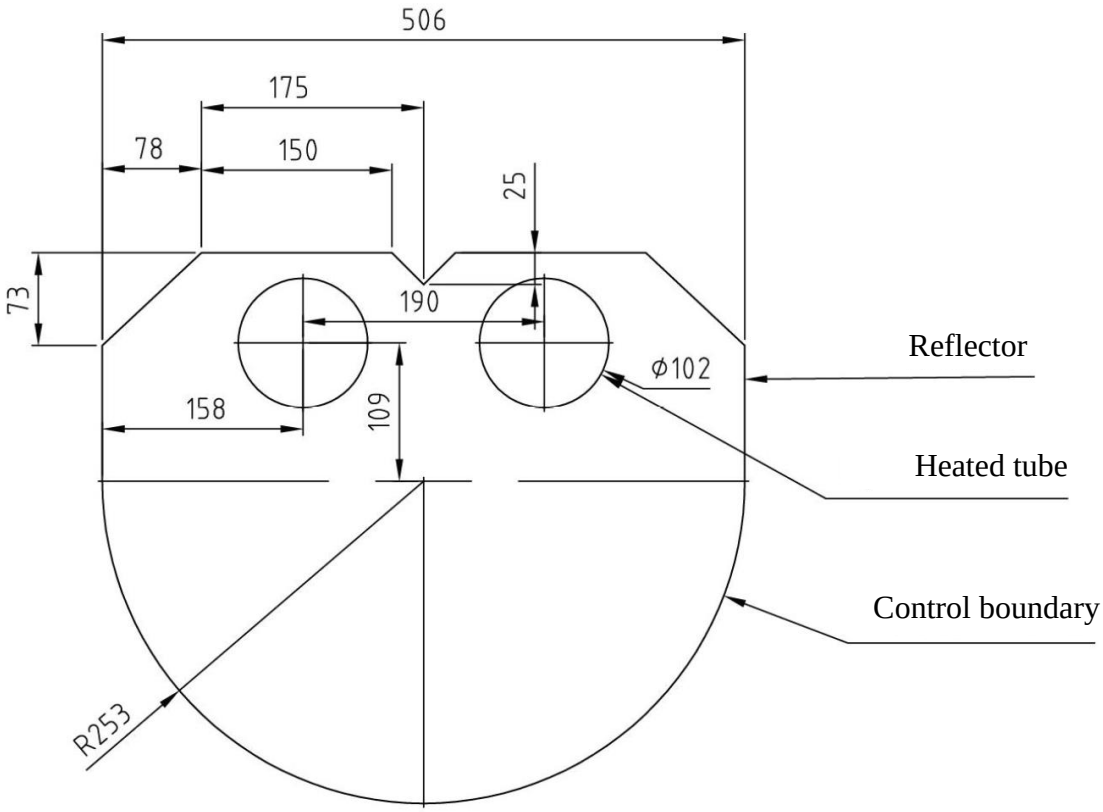

FIGURE 49. FIRST GEOMETRY OF REAL RADIANT HEATER

Figure 49 presents a 2D view of a U-shaped tube radiant heater. There are the two parts of the tube below the reflector. The reflector is shaped with straight lines and only in one part above both parts of the tube. A semi-circular control boundary is added for the simulation.

These tests were done as if the section was somewhere in the middle of the heater. Therefore, the temperatures were taken as 260 °C for the left part of the tube and 420 °C for the right part. The ambient temperature was taken as 25 °C and it was applied to the control boundary but also to the reflector to simplify the tests.

5.1. First series of tests

These tests were actually some preliminary tests, to find the correct setup of the parameters in Fluent to model the problem and to apprehend the study.

At start, the parameters not defined in the precedent part were kept the same as used for the tests with simple geometries. However, it appeared that this configuration led to inconsistent results (displayed on Figure 41). Indeed, the results obtained did not reflect the reality of the situation. The main incoherence involves the symmetry of the problem: the software produces a symmetrical result even though the configuration is asymmetrical (different temperatures for the two different parts of the tube). Some other problems can be noticed. The same strange pattern as before is observed around the tube and also on the control boundary. Moreover, here again the radiation only varies in a very small range as can be seen on the scale in Picture 50.

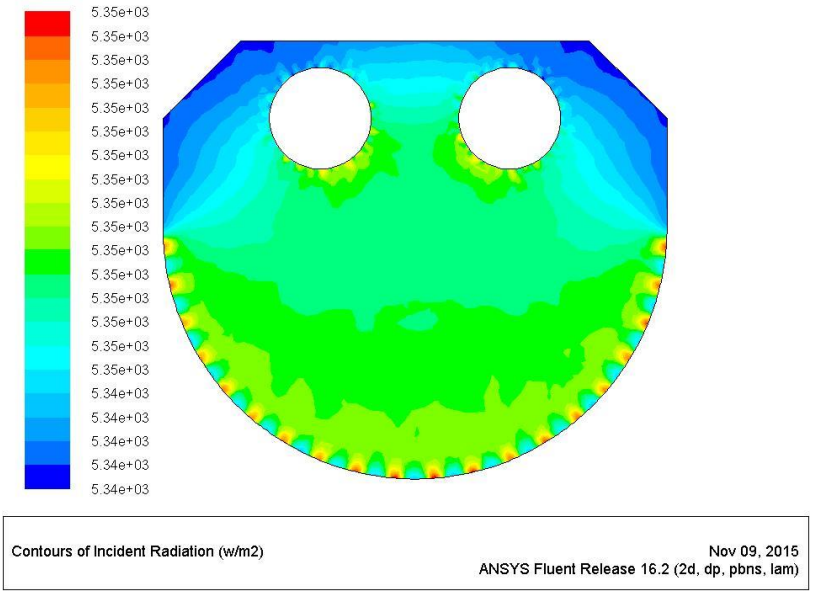

FIGURE 50. FIRST RESULTS FOR REAL GEOMETRY

With the results obtained, it can be seen that the configuration used here is not appropriate for the problem. Therefore, several modifications were tried. To better reflect the reality of the problem, the emissivities were changed to 0.2 for the reflector and 0.93 for the tube; for the control boundary, it was kept to 1. This modification alone did not improve the results but it was still kept because these values are closer to real values.

Increasing the temperature difference between the two parts of the tube was also tried to verify the symmetry problem. The results obtained were still symmetric even with a much higher temperature difference which attest that there was indeed a problem with the parameters themselves.

All the boundary conditions were defined by temperatures. This was thought to be able to lead to false results so the reflector boundary condition was changed to an adiabatic wall: defined by heat flux equal to 0. This modification had an influence on the results but did not affect the symmetry.

Finally, it was tried to use the coupled energy/DO model approach instead of the uncoupled. According to the Fluent manual, the main consequence of this approach is to speed up the simulation for certain cases involving high optical thicknesses or scattering coefficients but here it changed drastically the results. Realistic results were finally obtained as displayed on Figure 51. This time, the asymmetry of the problem can be observed as well as a wide range of incident radiation.

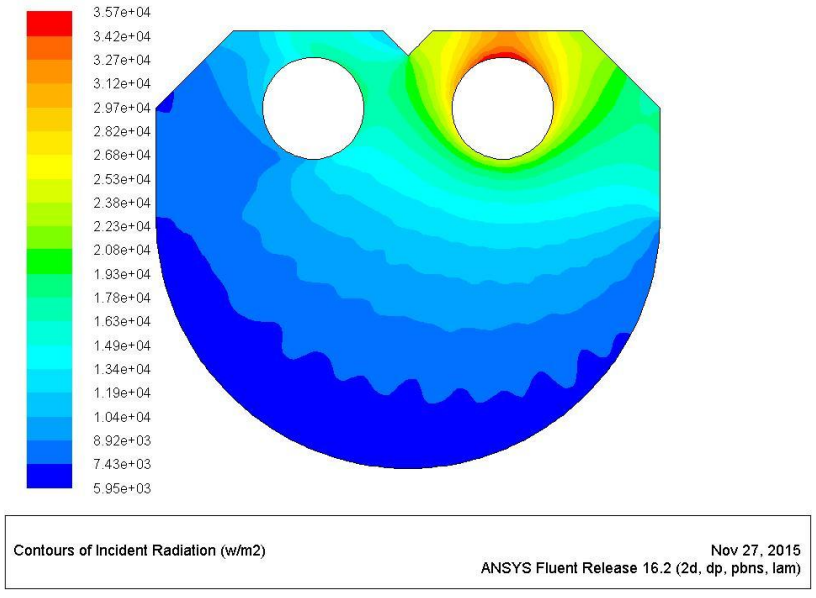

FIGURE 51. EXAMPLE OF RESULTS WITH COUPLED ENERGY/DO MODEL

Having found the configuration to use in Fluent to model the study, some tests were made to furtherly apprehend the problem. The surfaces were still taken as completely diffuse and opaque. Different angle discretizations and mesh sizes were used. For the reflector, both temperature-type and heat flux-type boundary conditions were tried. The incident radiation was

displayed on the control boundary in function of the angle of the arc from 0° to 180° and the results are presented on Figure 52.

It can be noticed that defining the reflector as an adiabatic wall (with a heat flux-type boundary condition) gives higher incident radiation overall. When changing only the way of defining the reflector from temperature to heat flux, the results were the same only shifted of several hundreds of W/m². This seems logical because this boundary condition means that the reflector is perfectly insulated so it should be giving higher radiation than if it is at ambient temperature. Moreover, it can be noticed that here the pixelation had no influence on the results. Therefore, in the following tests, the number of ϕ pixels is always fixed to 1.

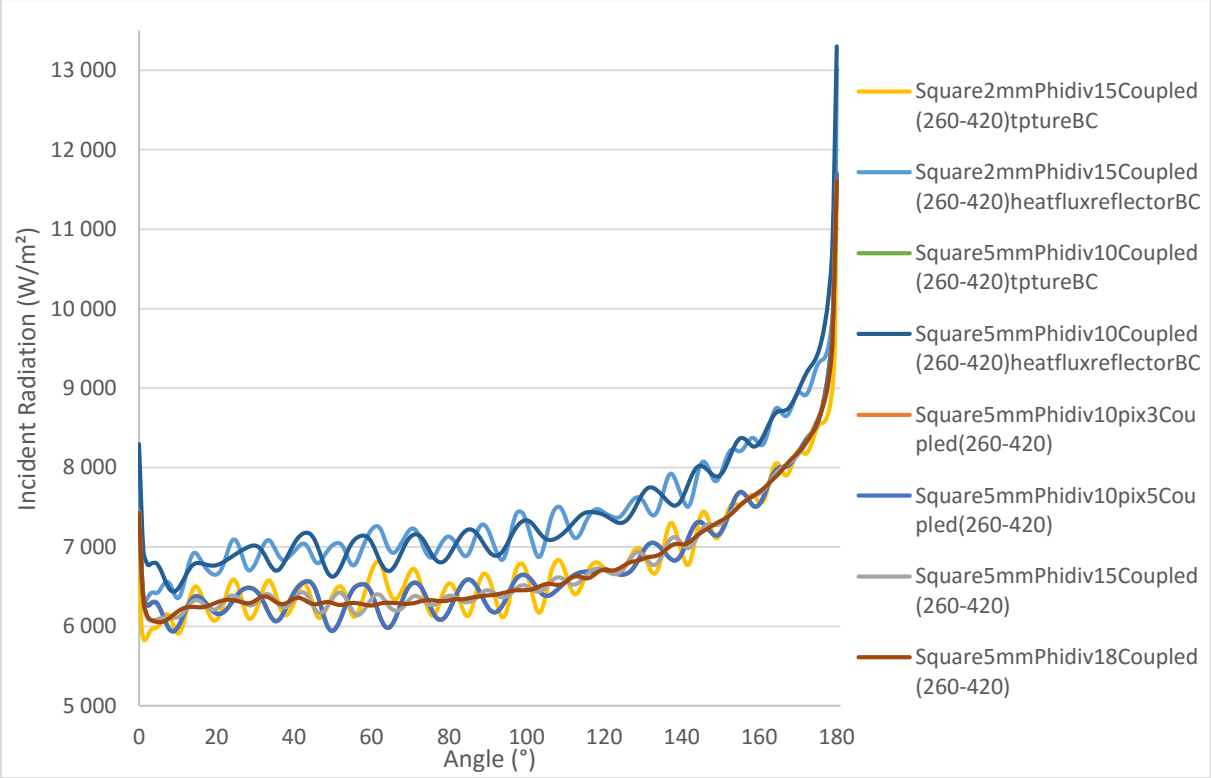

FIGURE 52. INCIDENT RADIATION ON THE CONTROL BOUNDARY FOR SURFACES OPAQUE AND DIFFUSE

5.2. Second series of tests

To be closer to the reality, the diffuse fraction of the reflector was here taken equal to 0.1. The reflector is indeed made of polished metal and therefore the reflected radiation on its surface is at 90% specular and only at 10% diffuse. Also and for the same reason, the control boundary was defined as permitted in the DO model as a semi-transparent wall instead of opaque. The reflector was defined by its temperature kept at 25°C.

12 tests were made where different mesh sizes and number of ϕ divisions were tried. As explained in the precedent chapter, the number of ϕ pixels was here kept to 1 for all the tests. 4 different mesh sizes were tested: 7 mm squares (3573 elements), 5 mm squares (6700 elements), 2 mm squares (41427 elements) and 1 mm squares (162300 elements). 3 different number of ϕ divisions are tried: 10, 15 and 18. For the finest mesh, only 10 and 15 ϕ divisions were tested: the simulation time was already very long and a higher number of ϕ divisions was not necessarily needed.

The results were studied the same way as before: the incident radiation was displayed as a function of the angle corresponding to the point. 11 curves were thus drawn. It can be observed on Figure 53 that for a same mesh size, increasing the number of ϕ divisions has a tendency to smooth the incident radiation. On the other hand, for a same angle discretization, refining the mesh leads a more oscillating incident radiation curve, as can be seen on Figure 54.

Refining the mesh does not seem to lead to a better solution due to the increasing of the number of peaks and their amplitude in the displayed incident radiation. This is explained by the nature of the angle discretization. Refining the mesh increases the number of elements on the boundary line. For the first mesh size, there was one ray in the angle discretization going through one cell, then for a finer mesh, there is some cells without rays. This phenomena gives rise to higher differences of value of radiation between two adjacent cells. Considering this, it seems that the incident radiation is not a good parameter to choose the density of the mesh and the angle discretization. With the displayed results, it is indeed impossible to draw some conclusion regarding the optimal set up.

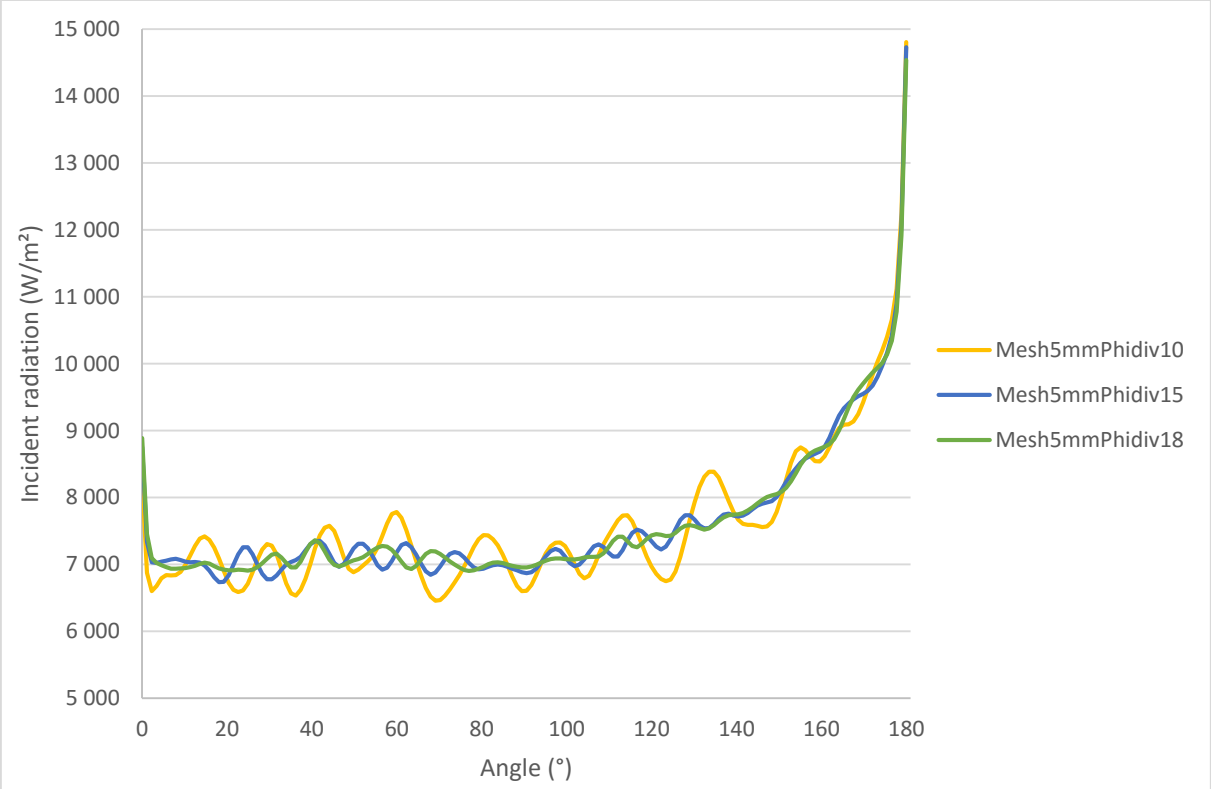

FIGURE 53. INCIDENT RADIATION FOR 5 MM SQUARES MESH

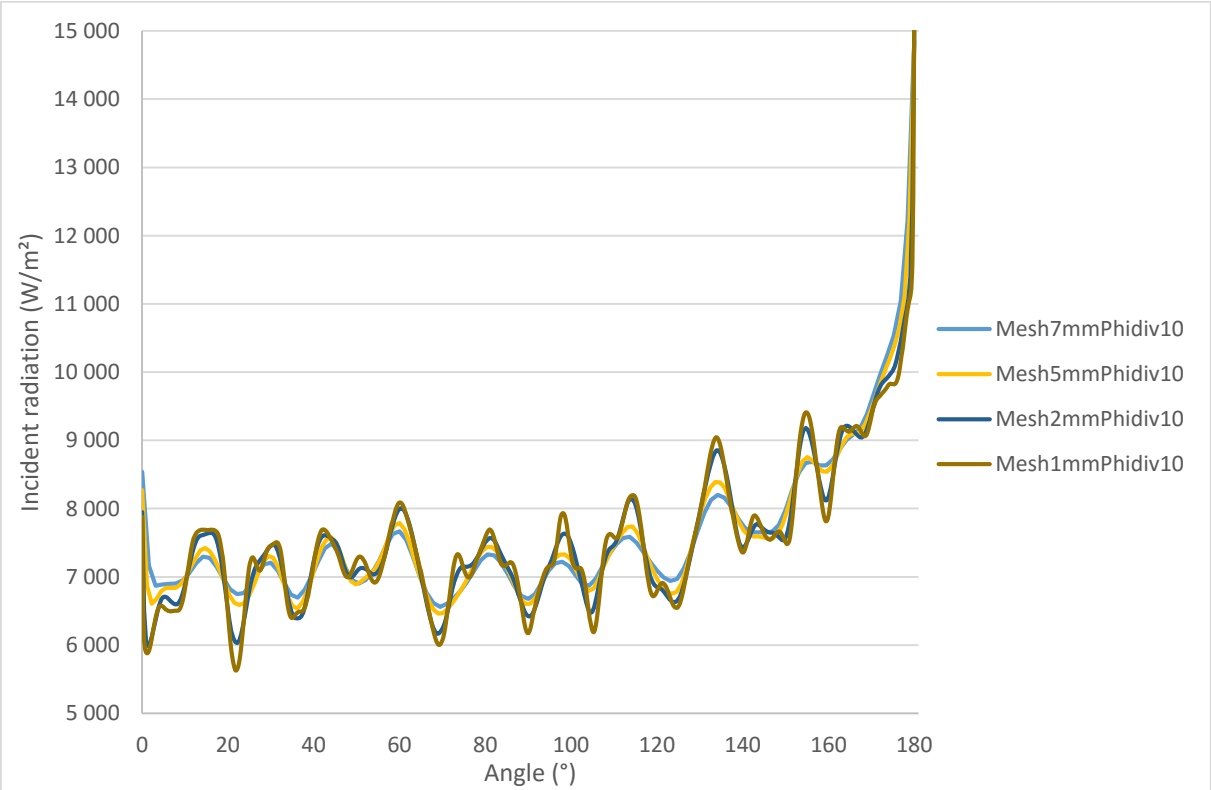

FIGURE 54. INCIDENT RADIATION FOR 10 ϕ DIVISIONS

5.3. Final decision on the configuration to use

In light of the precedent results, it was decided to consider the radiative heat flux rather than the incident radiation. This quantity was used to determine the mesh size and the angle discretization and it was also used later to compare the different heater geometries in the core of the study. It is indeed necessary to base the study on the same value that was used to determine the set-up of the problem to keep a consistency in the whole study. The contrary could lead to false results.

For this part, the tests of the precedent chapter were used.

To choose the mesh size, it is more precisely the total heat flux through a surface of 1 m depth on the control boundary that was studied here. The heat flux was calculated for each surface between two points of the data exported by Fluent based on the average value of the two incident radiation. Then these values were summed to obtain the total heat flux, which was compared for the different mesh sizes for the same angle discretization (15 ϕ divisions). A test for a 3 mm mesh was also added. The results are presented in Table 2.

TABLE 2. TOTAL HEAT FLUX FOR DIFFERENT MESH SIZES

Mesh size (mm) (square size)	7	5	3	2	1
Total heat flux (W)	6031	6019	6011	6002	5995
Heat flux change (W)		12	8	9	7
Heat flux change (% of precedent)		0.20	0.13	0.15	0.12

It is decided that if refining the mesh leads to a change of 0.2 % maximum in the total heat flux, then it can be said that the results are no longer dependant of the mesh size. In the light of the above table, it can be concluded that keeping the 7 mm mesh is enough since refining the mesh from this size does not lead to a change higher than 0.2 %. The final mesh size chosen is therefore a mesh of 7 mm squares, which corresponds for this geometry to 3573 cells.

It is especially interesting to keep a mesh that is not too fine because of the great consequences of the mesh size on the computation time. Indeed, for the chosen 7 mm mesh, it takes about 3 minutes to perform 100 iterations whereas for the 2 mm mesh it takes about 40 min so more than 10 times longer. This consideration obviously influences the choice of the mesh size.

To determine the angle discretization, the same method was used, comparing the total heat flux for different number of ϕ divisions. Here again, the chosen angle discretization is the one from where the results do not change for more than 0.2 % when increasing the angle discretization. The method chosen to do the comparison of different heater geometries in the core of the study demands a number of ϕ divisions multiple of 3 (see chapter 6.). Therefore, tests were performed with 6, 9, 12 and 15 ϕ divisions. The results are presented in Table 3.

TABLE 3. TOTAL HEAT FLUX FOR DIFFERENT ANGLE DISCRETIZATIONS

ϕ divisions	6	9	12	15
Total heat flux (W)	6069	6037	6029	6031
Heat flux change (W)		32	8	2
Heat flux change (% of precedent)		0.53	0.13	0.03

Considering this table, the value of 9 for ϕ divisions is chosen for the angle discretization.

In conclusion, the set up chosen for all the following tests is a uniform mesh of 7 mm squares. Concerning the angle discretization, default values are kept for θ divisions and pixels as they have no influence on the results. For the angle ϕ, the values of 1 for ϕ pixel and 9 for ϕ divisions are chosen. No surface is split.

6. Comparison of different geometries of tube radiant heater

6.1. Boundary conditions

The parameters used in these tests are similar to the ones used in the second set up tests with the first real geometry. All the surfaces boundary conditions were defined by their temperatures. The temperature of the control boundary was kept as 25 °C. However, the others were taken from real laboratory experiences using the heater from the manufacturer Kotrbatý. These measurements results are from the master thesis by Šubrt (2014). Temperatures were measured on the two parts of the tube and on different parts of the reflector, for three different sections: close to the burner, at the other extremity of the heater (far away from the burner, where the tube bends so the two parts of the tube are at the same temperature), and in the middle of these two sections. For this study, the temperatures of the first section, the one closest to the burner, were used. They are displayed in Table 4, and the corresponding surfaces are described in Figure 55.

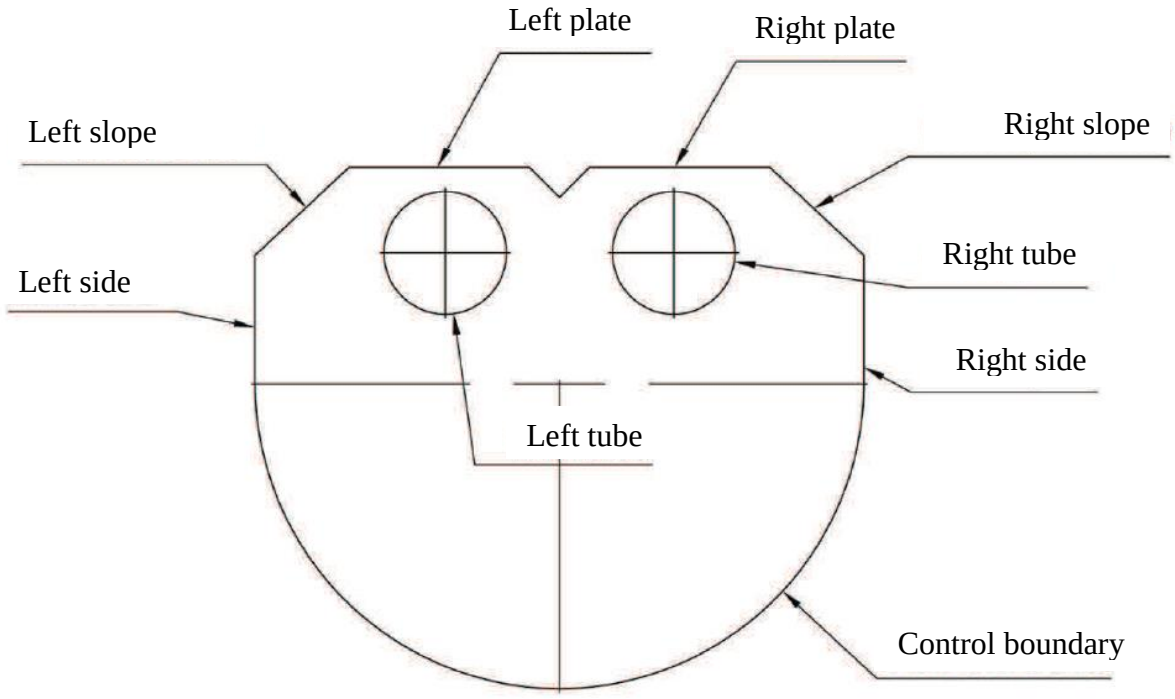

FIGURE 55. SURFACES DEFINITION FOR TEMPERATURE MEASURES [J. ŠUBRT (2014)]

TABLE 4. MEASUREMENTS OF TEMPERATURE ON A REAL HEATER

Surface	**Temperature (°C)**
Left tube	500
Right tube	180
Left side	90
Left slope	145
Left plate	200
Right plate	130
Right slope	97
Right side	65

To simplify the procedure, the simulations used only one temperature for the whole reflector, the same for all the heaters. A surface average temperature was calculated from the measured values and taken as the boundary condition at the reflector for all the heaters in the simulations.

$$T_{r,avg} = \frac{\sum S_k T_k}{\sum S_k} \tag{15}$$

The calculation gave the temperature of 129.5 °C.

The boundary conditions for the simulations were as showed in Table 5.

TABLE 5. BOUNDARY CONDITIONS FOR ALL SIMULATIONS

Surface	**Temperature (°C)**
Reflector	129.5
Tube 1 (left)	500
Tube 2 (right)	180
Control Boundary	25

6.2. Evaluation method

As said in chapter 4.3., the heat flux is used to evaluate and compare the different heaters. As before, it is calculated with a depth of 1 m. It would make no sense to compare the total heat flux on the control boundary because with different sizes of reflectors, there are different sizes of control boundaries. Therefore, the total heat flux varies also because of the size of the evaluation surface and no conclusion can be made on the efficiency of the heaters. Because of this, a more advanced method is used.

For a radiant heater, generally, a useful angle is defined at a value of 120° (see Figure 56). It corresponds to the directions where the people will be under the heater and where most of the heat produced by the heater is wanted. The heat received outside of this angle is arriving as such height and direction that it is considered useless.

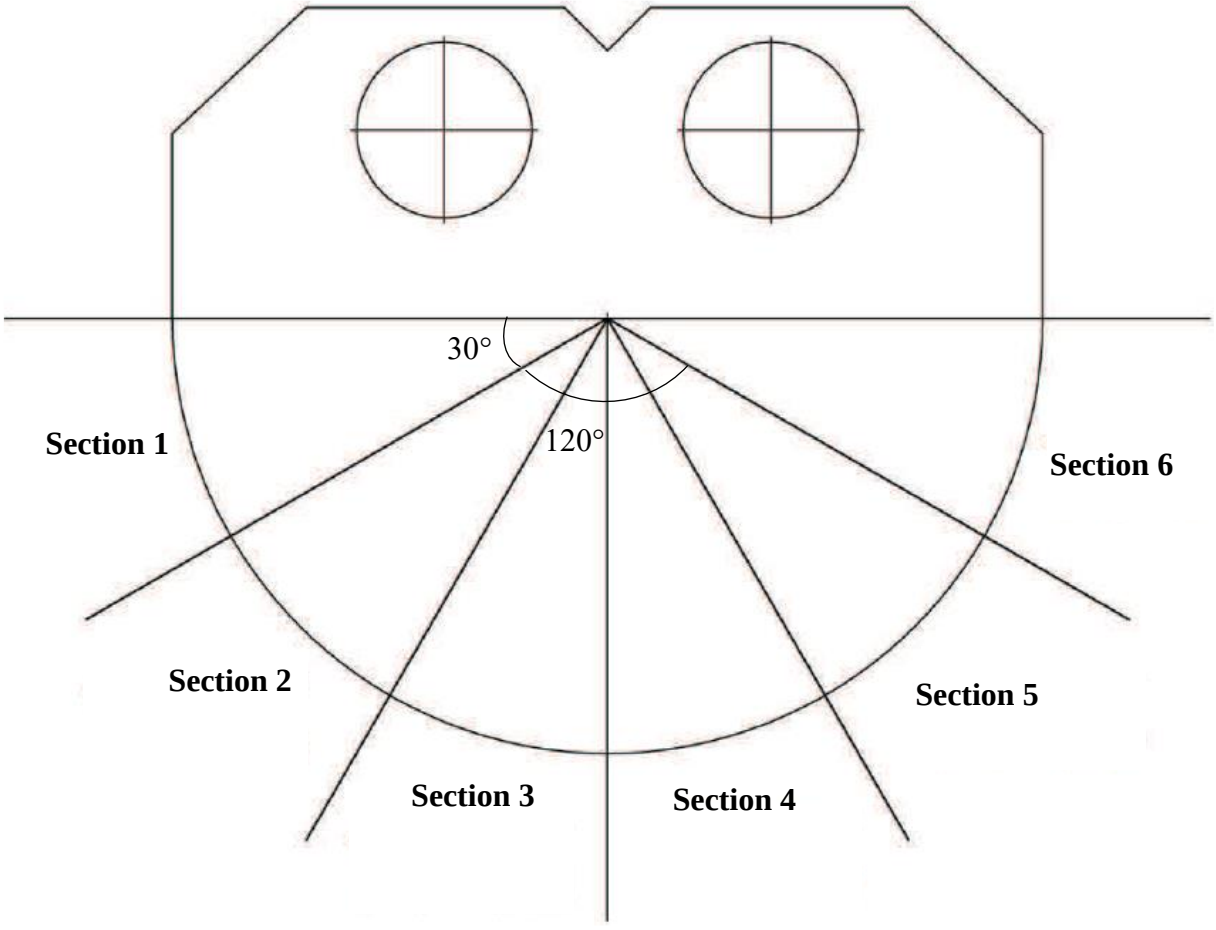

FIGURE 56. USEFUL ANGLE ILLUSTRATION

Therefore, for the comparison of the different geometries, the proportion of heat flux in the useful part and useless part is especially looked at. That is indeed what makes a good reflector geometry. It is its capacity to direct the heat in the useful angle.

To go further in the analysis, the repartition of the heat is detailed per section of the control boundary (see Figure 56). The partition between the left side and the right side is especially studied. Because of the great difference of temperature between the two parts of the tube, the left part of the control boundary clearly receives more heat than the right side. But the reflector shape has an influence on this repartition and can exacerbate or attenuate the difference between the two sides.

6.3. Simulations results

The simulations were conducted with the parameters described in the previous chapters. The coupled implementation for energy and DO model was chosen. For the comparison to make sense, the parameters were kept the same for all the geometries tested.

The incident radiation is displayed in Figures 57 to 63 to help visualize the simulations. As explained in the precedent part, the proportion of useful and useless heat was calculated for each geometry and the results are presented in Table 6.

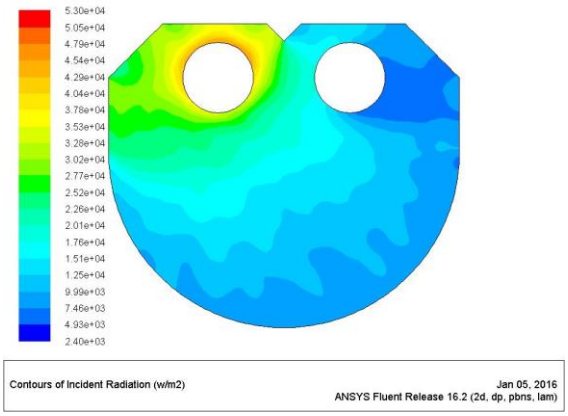

FIGURE 57. RESULTS FOR KOTRBATÝ KM

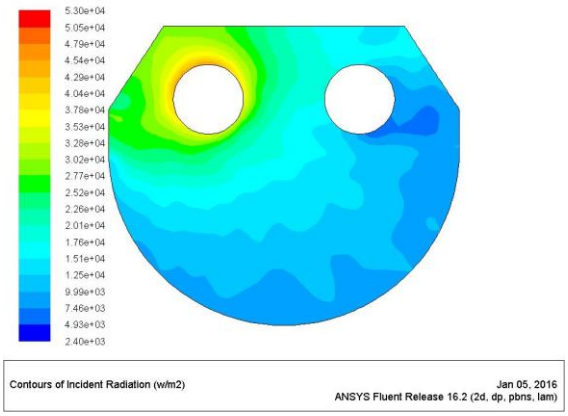

FIGURE 58. RESULTS FOR MANDÍK HELIOS 50

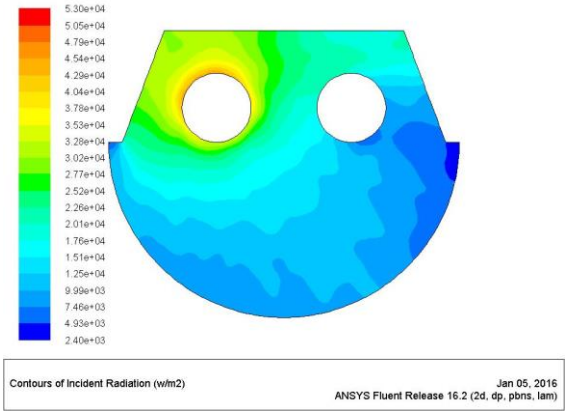

FIGURE 59. RESULTS FOR SCHWANK 50U

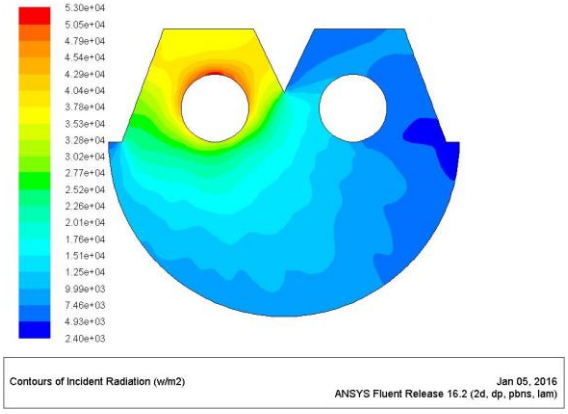

FIGURE 60. RESULTS FOR SCHWANK LL

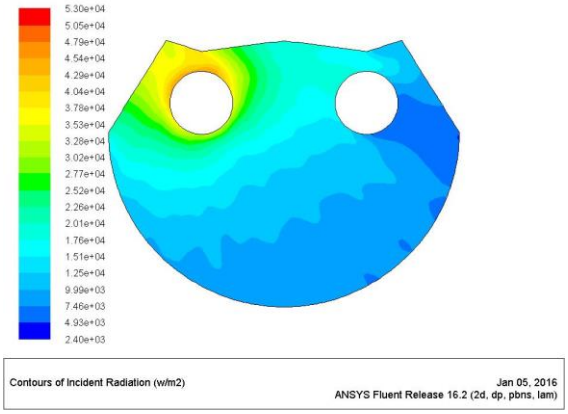

FIGURE 61. RESULTS FOR CARLIEUKLIMA MSC9

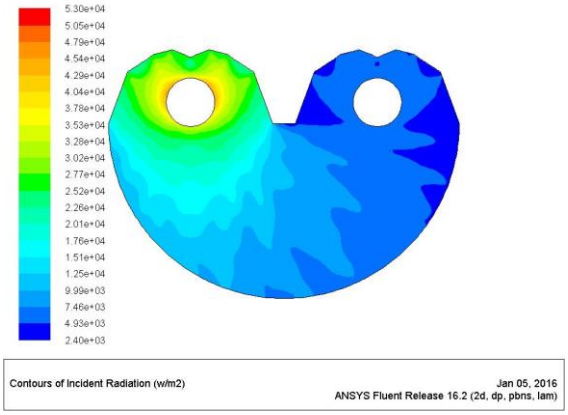

FIGURE 62. RESULTS FOR CARLIEUKLIMA MSU9

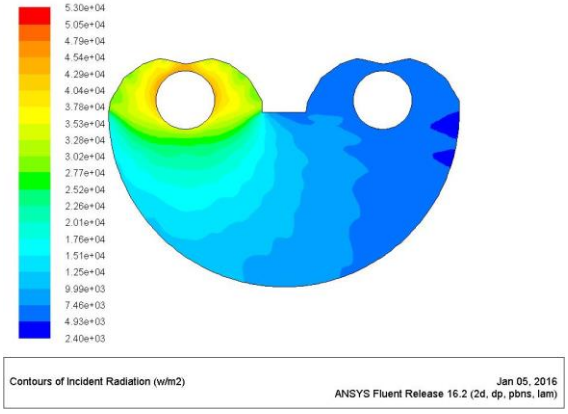

FIGURE 63. RESULTS FOR PAKOLE ZENIT 12

TABLE 6. RESULTS OF HEAT FLUX FOR DIFFERENT HEATERS

Model	Kotrbaty KM	Mandik Helios 50	Schwank 50U	Schwank LL	Carlieuklima MSC9	Carlieuklima MSU9	Pakole Zenit 12
Length (mm)	506	510	518	528	567	754	610
TOTAL hf (W)	7551	7670	6888	6877	7974	9373	9030
Useless (W)	2767	2830	2212	2160	2964	3173	3312
Useless (%)	37	37	32	31	37	34	37
Useful (W)	4784	4840	4676	4717	5010	6200	5718
Useful (%)	63	63	68	69	63	66	63

All heaters give between 63 % and 69 % of heat in the useful area defined in Figure 56.

The results show that the heaters from the manufacturer Schwank give the best ratio of useful and useless heat. Indeed they deliver almost 70 % of the heat in the useful area. From this point of view, they are the best heaters.

We can notice that the model LL has better results than the model 50U. Yet, the only difference between these two geometries is the semi-separation of the reflector between the two parts of the tube. Therefore it seems that this change of shape of the reflector improve the efficiency of the heater in terms of heat repartition in useful area.

The repartition of the heat flux per section of the control boundary is displayed on the graph of Figure 64 for the different geometries. The left/right partition is also detailed in the Table 7 for each geometry.

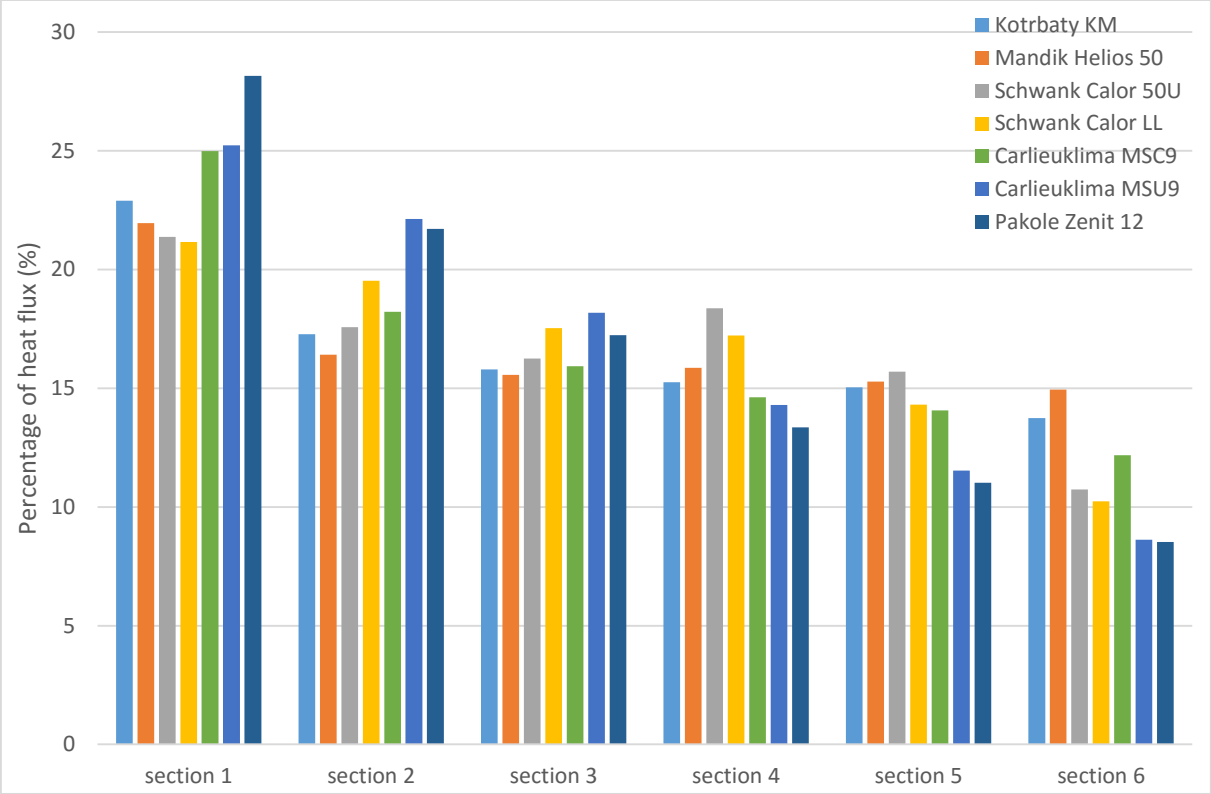

FIGURE 64. REPARTITION OF THE HEAT FLUX ON THE CONTROL BOUNDARY

TABLE 7. LEFT/RIGHT REPARTITION OF HEAT FLUX

Model	Kotrbaty KM	Mandik Helios 50	Schwank 50U	Schwank LL	Carlieuklima MSC9	Carlieuklima MSU9	Pakole Zenit 12
Heat to the left (%)	56	54	55	58	59	66	67
Heat to the right (%)	44	46	45	42	41	34	33

First of all, it can be noticed that there is indeed more heat on the left side of the heater than on the right side, because of the temperature difference between the left part and the right part of the tube.

The reflector that attenuates the most the difference of heat flux between the right part and the left part of the control boundary is the Mandik Helios 50. The Schwank 50U are also quite efficient. It can be noticed when looking at the geometries that both of them have a flat unbroken reflector above the tube. This feature helps to attenuate the difference in heat repartition between left and right. However, from the previous table, it was concluded that considering the

heat repartition between useful and useless area, it was actually better to have a small separation between the tubes on the reflector. It all depends on what the designer find the most important.

The results show that reflectors in two separated parts increase the difference of heat between the two sides of the heater. Only less than 35 % of the heat is on the cold side for both geometries with separated reflector whereas for all of the others, the value is above 40 %.

For the Pakole heater, almost 30 % of the total heat flux is located on the section 1 (leftmost section, see Figure 56). This section is indeed the closest one the hottest part of the tube but the reflector task is precisely to properly redirect the heat. It is especially a problem because this section is in the useless part of the heat distribution.

These results can be especially interesting for designers of heating systems. Indeed, they can provide a big help to choose the configuration of several heaters in a room. Substantially more heat is transferred to the side of the tube attached to the burner and this information has an influence on the way to arrange heaters in the room. For instance, it could be advantageous to place the heaters in inverse configurations to counteract the problem of heat repartition.

Considering Tables 6 and 7, the best heater seems to be the model Schwank 50U. It offers the best compromise between the two repartitions studied.

7. Conclusion

In this study, the influence of tube radiant geometry on the distribution of emitted heat radiation was analysed. Some preliminary tests were conducted to apprehend and study the discrete ordinates model in Fluent. Particularly the influences of angle discretization, density of the numerical grid and surface splitting were tested. To do this, two simple geometries and the real geometry of one heater from a manufacturer were used.

This helped to decide about some main parameters to use in Fluent for the further simulations. Surface splitting was found not important in this problem. For the angle discretization a number of 9 ϕ-divisions and of 1 ϕ-pixel were chosen. The selected numerical grid was a mesh of 7 mm squares. An important finding was that for these simulations it was necessary to select the coupled implementation of energy transport and discrete ordinates model. Thanks to these preliminary tests, it was also found that incident radiation was not a suitable parameter for this study. The radiative heat flux was used instead for the decision on the configuration and for the comparison of heaters.

Seven heaters found on the market were compared. It was chosen to focus on the reflector geometry and only this feature of the heaters was compared. A method was found to evaluate the effectiveness of the different heaters using the radiative heat flux. The control boundary was split into several sections; the radiative heat flux was evaluated on each section. The partition based on the useful angle of the heater and the partition between left and right part of the heater were especially studied.

Considering the heaters comparison, the study provided some useful information for designers of heating system using tube radiant heaters. The heat flux quantity was displayed on each section for each heater which offers a visual comparison of the heaters. Considering the heat distribution on the useful angle, the best heaters from the seven tested were those from the manufacturer Schwank. They were the ones delivering the greatest amount of heat in the useful angle of the heater, meaning in the user's direction. The reflector that was found to attenuate the most the difference of heat flux between the right part and the left part of the control boundary was the Mandik Helios 50. Coupling both considerations, the best heater seemed to be the Schwank 50U.

This work was done using temperature-defined boundary conditions for all elements of the heater. All the temperatures on the boundaries were taken thus considered constant. If it is almost realized on the tube, on the reflector it is a rough approximation. An improvement of this study could be to take into consideration the convection occurring on the external side of the reflector during the real operation of the heater. Subsequently, the model could also integrate some insulation on the reflector and study its influence. From there, several types of insulation could be compared.

It could also be interesting to study the influence of the reflector material properties on the heat distribution. In the current work, the diffuse fraction of the reflector was taken equal to 0.1. However, this value depends on the chosen material and it is also increasing with the time of utilisation of the heater. As the reflector becomes more and more diffuse, the heat distribution is changed. The best reflector geometry might not be the one selected here when using a higher diffuse fraction. This consideration can be important when choosing a tube radiant heater because it gives information on its long-term use.

In this study, all the simulations were done in two dimensions, at the part of the heater closest to the burner. It would be interesting to go further by doing a 3-D simulation of the whole radiant heater. The flame and tube lengths would thus be taken into account. The ratio of the flame length on the tube length has a particularly important role on the heat distribution in the third dimension of the problem. To compare several heaters in 3-D, it would be useful to have some information on the flame length by some measurements or from manufacturer information. Otherwise, some different values could be tested to study the influence of this ratio on the different heaters.

8. References

Siegel R., Howell J. (2002), *Thermal Radiation Heat Transfer.* 4th ed. Taylor & Francis, New York.

Modest M. F. (2003), *Radiative Heat Transfer.* 2nd ed. Academic Press, London.

ANSYS Inc. (2015), *ANSYS Documentation, Release 16.2.*, Canonsburg.

Fluent Inc. (2006), *FLUENT User's Guide, Release 6.3*.

Lienhard J. IV, Lienhard J. V (2008), *A Heat Transfer Textbook.* 3rd ed. Phlogiston Press, Cambridge.

Šubrt J. (2014), *Sálání tmavých plynových zářičů (Heat radiation of tube radiant heaters)* [master thesis]. CTU in Prague, Faculty of Mechanical Engineering.

Henderson T. (2015), *The Physics Classroom* [available on-line] www.physicsclassroom.com, visited on 07/01/2016.

Schwank (2015), *Schwank Documentation*, [available on-line] www.schwank.de, visited on 20/11/2015.

Kotrbatý V.M.Z., spol. s r.o., [available on-line] www.kotrbaty.cz, downloaded on 30/11/2015

Mandík a.s., [available on-line] www.mandik.cz, downloaded on 30/11/2015

Carlieuklima SpA, [available on-line] www.carlieuklima.com, downloaded on 30/11/2015

Schwank CZ, s.r.o., [available on-line] www.schwank.cz, downloaded on 30/11/2015

Pakole Trade Kft., [available on-line] www.pakole.hu, downloaded on 30/11/2015